eLIFE elifesciences.org

RESEARCH ARTICLE

Live imaging of heart tube development in mouse reveals alternating phases of cardiac differentiation and morphogenesis

Kenzo Ivanovitch†, Susana Temiño, Miguel Torres*

Developmental Biology Program, Centro Nacional de Investigaciones Cardiovasculares, Madrid, Spain

Abstract During vertebrate heart development, two progenitor populations, first and second heart fields (FHF, SHF), sequentially contribute to longitudinal subdivisions of the heart tube (HT), with the FHF contributing the left ventricle and part of the atria, and the SHF the rest of the heart. Here, we study the dynamics of cardiac differentiation and morphogenesis by tracking individual cells in live analysis of mouse embryos. We report that during an initial phase, FHF precursors differentiate rapidly to form a cardiac crescent, while limited morphogenesis takes place. In a second phase, no differentiation occurs while extensive morphogenesis, including splanchnic mesoderm sliding over the endoderm, results in HT formation. In a third phase, cardiac precursor differentiation resumes and contributes to SHF-derived regions and the dorsal closure of the HT. These results reveal tissue-level coordination between morphogenesis and differentiation during HT formation and provide a new framework to understand heart development.
DOI: https://doi.org/10.7554/eLife.30668.001

***For correspondence:** mtorres@cnic.es

Present address: †The Francis Crick Institute, London, United Kingdom

Competing interests: The authors declare that no competing interests exist.

Funding: See page 26

Received: 23 July 2017
Accepted: 26 November 2017
Published: 05 December 2017

Reviewing editor: Richard P Harvey, Victor Chang Cardiac Research Institute, Australia

Introduction

The heart is the first organ to form and function during embryonic development. At embryonic day (E) 7.5, cardiac precursors in the splanchnic mesoderm (mesoderm apposed to the endoderm) differentiate into cardiomyocytes by assembling the contractile sarcomere machinery (***Tyser et al., 2016***) and form a bilateral structure known as the cardiac crescent (cc) in the mouse. Concomitant with foregut invagination, the cc swings inwards to become placed underneath the developing head folds. By a complex morphogenetic process, the cc subsequently transforms into an early heart tube (HT) initially opened dorsally, which by E8.25 has transformed into a closed and beating linear HT, also known as the primitive HT (***Evans et al., 2010***; ***Kelly et al., 2014***).

The cc and early HT mainly give rise to the left ventricle (***Zaffran et al., 2004***). The right ventricle (RV), the outflow tract and most of the atria derive instead from cardiac progenitors located dorsomedially to the cc in the splanchnic mesoderm, that are progressively recruited at the poles of the HT at subsequent developmental stages (***Cai et al., 2003***; ***Kelly et al., 2001***; ***Mjaatvedt et al., 2001***; ***Waldo et al., 2001***; ***Galli et al., 2008***). These findings led to the concept that cardiac mesodermal progenitors contain two populations of cells: the first heart field (FHF) precursors, recruited early in development to form the initial HT and mostly containing the LV primordium, and the second heart field (SHF), recruited later and elongating the HT (***Buckingham et al., 2005***).

Clonal analysis (***Devine et al., 2014***; ***Lescroart et al., 2014***; ***Meilhac et al., 2004a***) supports the idea that FHF and SHF precursors are two independent developmental fields with dedicated molecular pathways. Clonal analysis also showed that the SHF shares a common origin with the skeletal muscles of the head and neck within the pharyngeal mesoderm (***Lescroart et al., 2010***; ***Lescroart et al., 2015***), further supporting differences between FHF and SHF populations. However, the existence of a common precursor between FHF and SHF was also reported in the early mouse

eLife digest We all start life as a single cell, which – over the course of nine months – multiplies to generate the billions of cells that can be found in a newborn. As an embryo develops, the cells need to achieve two major tasks: they need to diversify into different types of cells, such as blood cells or muscle cells, and they need to organize themselves in space to form tissues and organs.

The heart of an embryo, for example, first forms a simple structure called the heart tube that can pump blood and later develops into the four chambers that we see in adults. The tube is made up of cells from two different origins, known as the first and second heart fields. Unlike other organs, the heart has to start beating while it is still developing, and until now, it was unclear how the heart manages this difficult task.

Here, Ivanovich et al. studied mouse embryos grown outside the womb by using a combination of advanced microscopy and genetic labeling to track how single cells turn into beating cells and move while the heart forms. The results showed that specializing into beating cells and forming the heart tube shape happened during alternating phases. The first heart-field cells turned into beating cells and began to contract at an early stage before the heart tube was formed. Next, the cells of the second heart field did not instantly develop into beating cells, but instead, helped the first heart-field cells to acquire the shape of a heart tube. Once this was completed, the second heart-field cells started to specialize into beating cells and created the additional parts of the more complex adult heart.

This research shows that the second heart field plays an active role in helping the heart tube form. The alternating phases of cell specialization and tissue formation allow the heart to become active whilst it is still developing. A better insight into how the heart forms may help us to create new treatments for various genetic heart conditions. The methods used here could also help to study how cells build other organs.

DOI: https://doi.org/10.7554/eLife.30668.002

embryo (***Meilhac et al., 2004a***) and other views suggest that the heart would form by a continuous differentiation process from a single population of cardiac precursors and only timing of recruitment would distinguish cells of the FHF and SHF (***Abu-Issa et al., 2004***; ***Moorman et al., 2007***). In support of the latter, the typical marker of the SHF, Islet1 (***Cai et al., 2003***), is also transiently expressed in FHF precursors and must therefore be considered as widespread cardiac progenitor marker instead (***Cai et al., 2003***; ***Prall et al., 2007***; ***Yuan and Schoenwolf, 2000***). Whether the recruitment of cardiomyocytes from progenitors is a continuous process and how this coordinates with morphogenesis, however, has not been directly studied. This is partly because the spatial arrangement of progenitors and differentiated cardiomyocytes has so far been analyzed on fixed embryos (***Cai et al., 2003***; ***Später et al., 2013***) and the expression dynamics of genes reporting differentiation together with cell movements during HT morphogenesis have not been captured so far (***Abu-Issa, 2014***).

Here, we report the live-imaging and 3D+t cell tracking of HT formation in whole mouse embryos. Using this method, in conjunction with an Nkx2.5eGFP reporter line, which provides high level of GFP in differentiated cardiomyocytes, we studied the dynamics of cardiac field differentiation. During an initial phase, FHF cardiac precursors differentiate rapidly to form a cardiac crescent, while limited morphogenesis takes place. During a second phase, no differentiation events are detected and extensive morphogenesis, including splanchnic mesoderm sliding over the endoderm, results in HT formation. Finally, using an Isl1-Cre lineage-tracing assay combined with live-imaging, we show that during a third phase, cardiac precursor differentiation resumes and contributes not only to the known SHF-derived regions but also to the dorsal aspect of the HT. These results show essential properties of FHF and SHF contribution to heart development and reveal tissue-level coordination between alternating phases of differentiation and morphogenesis during HT formation.

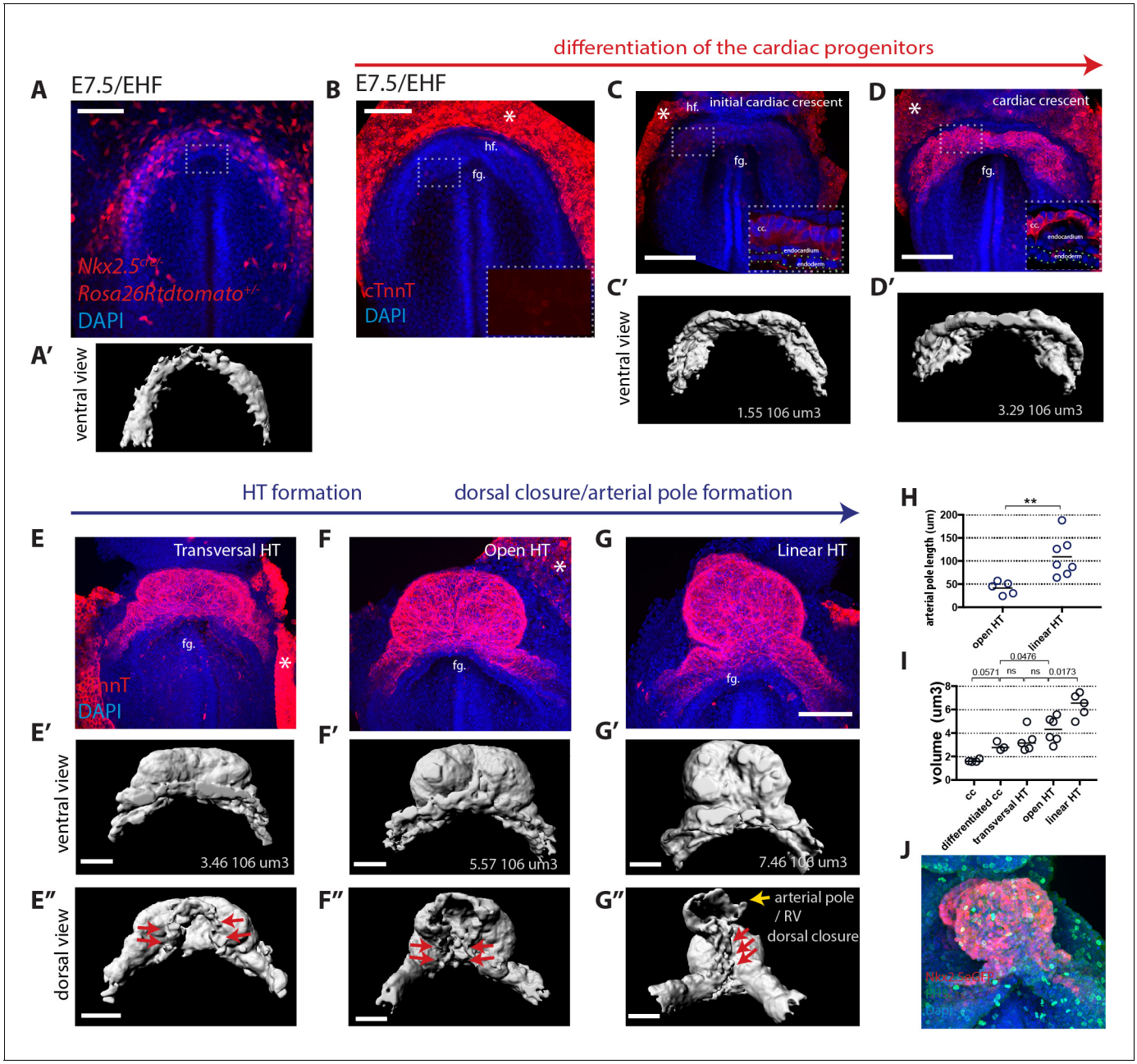

Figure 1. Overview of HT morphogenesis and growth. (**A**) Frontal view of an *Nkx2.5$^{cre/+}$; Rosa26Rtdtomato* embryo at EHF stage. (**A'**) 3D reconstruction of the tdtomato signal in the cardiogenic area. Signal from tdtomato+ endothelial cells identified by shape was manually masked. See also ***Video 1***. (**B–G**) Immunostaining for cTnnT (red) and Dapi (blue) showing six consecutive stages during cardiac differentiation (**B–D**) and HT morphogenesis (**E–G**). (**B**) At EHF cTnnt is initially not detectable. (**C–D**) During early somitogenesis, cTnnT signal becomes detectable in the cc. Insets in (**B–D**): magnification of single optical sections showing cTnnT localization and cell shape. (**C'–G' and E''–G''**) Corresponding 3D renderings from cTnnT signal reconstruction. Red arrows in (**E'–G'**) highlight the dorsal closure of the HT. Yellow arrow in G'' highlights the arterial pole (prospective RV). See also ***Video 2***. (**H**) Quantification of the arterial pole/RV length in the open HT (41.4 ± 14.0 µm, n = 5) and after dorsal closure (109 ± 43.44 µm, n = 7), mean ±SD, p=0.0025. (**I**) Quantification of the cardiac volume at the different stages of HT development. (Initial cc: 1.63.106 µm3 ± 0.13, n = 4, cc: 2.89.106 ± 0.37 µm3, n = 3, transversal HT: 3.367. 106 µm3 ± 0.95, n = 5, open HT: 4.29.106 µm3 ± 1.08, n = 6, linear HT: 6.37. 106 µm3 ± 1.01, n = 5, mean ±SD). p-Values are indicated on the graph. (**J**) Immunostaining of an *Nkx2.5eGFP* embryo for PH3 (red) and Dapi (blue) at HT stage, showing proliferative cells in the ventricle. Scale bars: 100 µm.

DOI: https://doi.org/10.7554/eLife.30668.003

The following source data and figure supplements are available for figure 1:

Source data 1. Source data for ***Figure 1H and I***.

Figure 1 continued on next page

Figure 1 continued

DOI: https://doi.org/10.7554/eLife.30668.007

Figure supplement 1. Criteria for embryo staging.

DOI: https://doi.org/10.7554/eLife.30668.004

Figure supplement 2. Lineage tracing using the *Nkx2.5^{cre}* driver shows a contribution of labeled cells to the cardiogenic regions but not to the endoderm at EHF stage.

DOI: https://doi.org/10.7554/eLife.30668.005

Figure supplement 3. Faint cTnnT signal starts to be detected at EHF stage in apico-basally polarized cc cells.

DOI: https://doi.org/10.7554/eLife.30668.006

Results

3D static analysis of mouse HT formation

To assess how the initial cardiogenic region transforms into a HT and differentiates, we first analyzed *Nkx2.5$^{cre/+}$; Rosa26Rtdtomato$^{+/-}$*embryos, in which both cardiac precursors and cardiomyocytes are labeled (***Stanley et al., 2002***). Before cc differentiation, at early head fold stage (EHF, ~E7.5), the cardiogenic region is visualized as a flat horse shoe-shaped tdtomato+ mesodermal layer at the rostral border of the embryo (***Figure 1A,A'***, and ***Video 1***). ***Figure 1—figure supplement 1*** shows the criteria for embryo staging (***Downs and Davies, 1993***; ***Lawson and Wilson, 2016***). In the *Nkx2.5$^{cre/+}$; Rosa26Rtdtomato$^{+/-}$* embryos, tdtomato labeling is also observed in the endocardium and endothelial cells (***Stanley et al., 2002***) but not in the endoderm (***Figure 1—figure supplement 2A,A'***). We next studied the distribution of Cardiac troponin T (cTnnT), one of the first evident sarcomeric proteins to appear in the cardiac crescent (***Tyser et al., 2016***). At EHF stage (***Figure 1B***), while most embryos are negative for cTnnT expression, some embryos show weak cTnnT localization in subsets of cells (***Figure 1—figure supplement 3A,A'***). At a subsequent embryonic stage (~E7.7), cTnnT signal reveals the cc, which is folding inwards. During folding, the cTnnT signal increases. cTnnT+ cells are initially columnar epithelial cells and show apical localization of the tight junction component zona-occluden-1 (ZO-1) (***Figure 1—figure supplement 3B,B'***). During differentiation, cardiac precursors switch to a rounded shape (***Linask et al., 1997***) (***Figure 1C,D***) and separate from the endoderm, while maintaining a basal lamina at the endocardial side (inset in ***Figure 1D*** and ***Figure 2D***). Morphogenetic changes starting at ~E8 subsequently lead to the formation of a hemitube whose major axis is transversal to the embryo A-P axis. We will refer to this stage as transversal HT (***Figure 1E***). Later, the tube adopts a more spherical shape, very similar to the linear HT but still open dorsally. We will refer to this stage as open HT (***Figure 1F***). The HT eventually closes dorsally (***Figure 1G***, red arrows in ***Figure 1G''***) and a prominent arterial pole (prospective RV) (***Zaffran et al., 2004***) becomes visible, completing linear HT formation by ~E8.25 (yellow arrows in ***Figure 1G''***, ***Figure 1H***, see also ***Video 2***).

To assess the overall growth of the forming HT, we measured cTnnT+ tissue volume in segmented z-stacks, at the stages described above (***Figure 1I*** and ***Figure 1—source data 1***). During the first phase of cardiomyocyte differentiation, the cTnnT signal expands resulting in a cardiac crescent rapidly doubling in volume (***Figure 1C', D', I***). During the subsequent phase of morphogenesis, from cc to open HT stage, growth is less pronounced despite extensive morphological changes (***Figure 1E', F', I***). The volume of the HT appears to increase again upon addition of the RV primordium to the arterial pole and dorsal HT closure (***Figure 1G', I***). HT growth likely reflects an increase in cell number occurring during the formation of the heart tube. Cardiomyocytes are proliferative at this stage (***de Boer et al., 2012***), and we can indeed observe mitotic figures in the HT (***Figure 1J***). From this analysis, however, it is

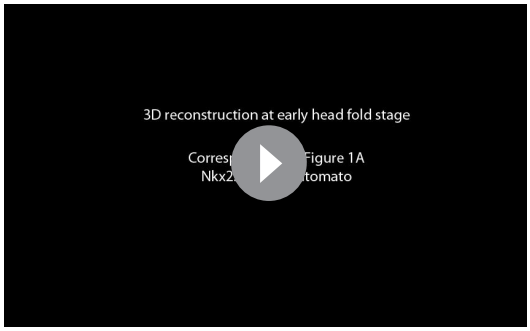

Video 1. 3D reconstruction of the cardiac crescent at EHF stage, based on *Nkx2.5$^{cre/+}$Rosa26Rtdtomato$^{+/-}$* signal. Related to ***Figure 1A***.

DOI: https://doi.org/10.7554/eLife.30668.012

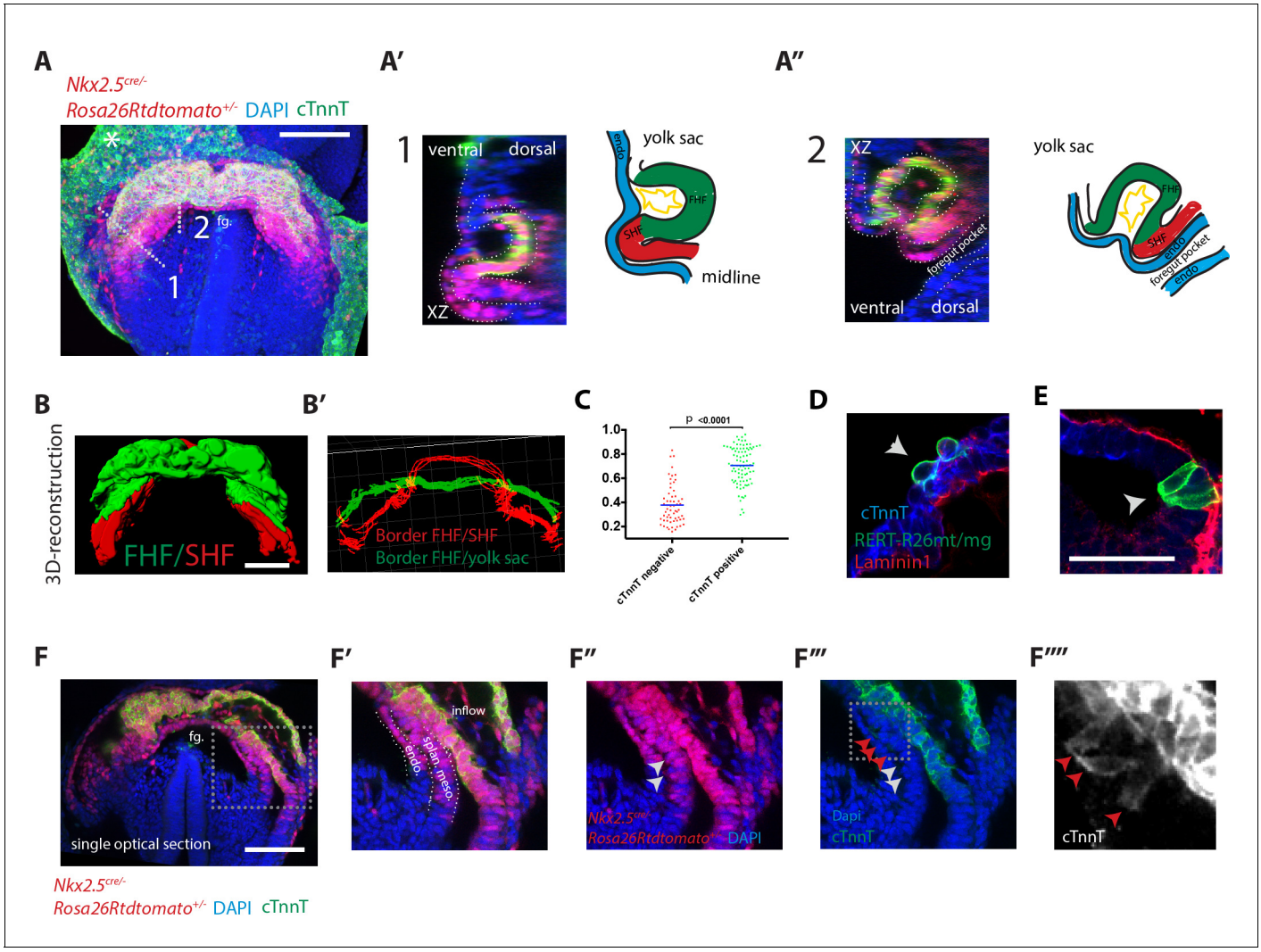

Figure 2. Visualization of the boundary between FHF and SHF. (**A–A″**) An *Nkx2.5$^{cre/+}$; Rosa26Rtdtomato$^{+/-}$* embryo immunostained for cTnnT (green) and Dapi (blue) showing cells of the Nkx2.5+ lineage populating both the FHF and SHF. (**A′ and A″**) Cross-sections in xz along the dotted lines 1 and 2 shown in (**A**), and corresponding schematics highlighting the endoderm (blue), FHF (green), SHF (red) and endocardium (yellow). Note that tdtomato signal is also detected in the endoderm and endocardium. (**B**) 3D reconstruction of the FHF (green) and SHF (red); (**B′**) 3D drawing of the border between the FHF and SHF (in red) and the FHF and yolk sack (in green) (based on the embryo shown in (**A**). For SHF rendering, the tdtomato+ splanchnic mesoderm was depicted. The FHF was rendered using the cTnnT signal. See also ***Video 3***. (**C**) Quantification of the cell roundness (rnd) index of cardiomyocytes at HT stage on single optical sections. Black bars indicate mean. Rnd index for cTnnT+ (green) cells is 0.71 ± 0.16 and for cTnnT- (red) cells is 0.38 ± 0.16, mean ±SD, exact p value < 0.0001. (**D–E**) Membrane-GFP labeling of typical cTnnT +FHF (**D**) and cTnnT-SHF (**E**) cells at longitudinal HT stage. The specimen is immunostained for cTnnT (blue), the basement membrane marker Laminin1 (red) and GFP (green). (**F**) Single optical section of the same embryo shown in (**A, B**). (**F′–F‴**) Inset: red arrows point to cells localizing weak cTnnT signal and have columnar cell shape in the SHF. White arrows point to cTnnT-negative SHF cells. splan. meso: splanchnic mesoderm, endo: endoderm, fg: foregut. In all the embryos immunostained for cTnnT, the yolk sack signal is non-specific background (indicated by an asterisks). Scale bars: 100 μm except in (**D–E**): 50 μm.

DOI: https://doi.org/10.7554/eLife.30668.008

The following source data and figure supplements are available for figure 2:

Source data 1. Source data for ***Figure 2C***.

DOI: https://doi.org/10.7554/eLife.30668.011

Figure supplement 1. Image segmentation of the FHF and SHF.

DOI: https://doi.org/10.7554/eLife.30668.009

Figure supplement 2. Endocardium localization in the cardiac crescent.

DOI: https://doi.org/10.7554/eLife.30668.010

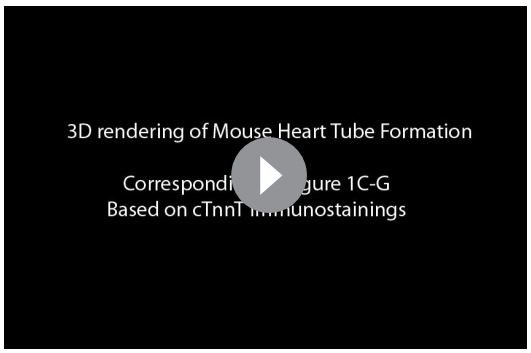

Video 2. 3D reconstruction of Mouse HT formation, based on embryos immunostained for cTnnT. Five representative stages are represented. Related to ***Figure 1C–G***.
DOI: https://doi.org/10.7554/eLife.30668.013

Video 3. 3D reconstruction of the FHF (green) and SHF (red). Based on *Nkx2.5$^{cre/+}$Rosa26Rtdtomato$^{+/-}$* embryos immunostained for cTnnT. The border between cTnnT-negative and cTnnT-positive cells can be visualized at the interface between the red and green domains. Related to ***Figure 2B***.
DOI: https://doi.org/10.7554/eLife.30668.014

unclear how much of the growth observed is due to cardiomyocyte proliferation versus addition of new cardiomyocytes from cardiac progenitor cells located in the splanchnic mesoderm.

3D analysis of cardiac progenitor differentiation

To visualize the boundary where cardiac progenitors abut differentiating cardiomyocytes during HT morphogenesis, we immunostained *Nkx2.5$^{cre/+}$Rosa26Rtdtomato$^{+/-}$* embryos at the transversal-HT stage with the differentiation marker cTnnT and acquired whole-mount images (***Figure 2A***). Cre activation of tdtomato was detected in both the FHF and SHF, as well as in the endoderm and endocardium (see optical sections in ***Figure 2A', A'', F,F'*** and ***Figure 2—figure supplement 1A***) (***Stanley et al., 2002***). Cardiomyocytes are separated from the endoderm by the endocardium. In contrast, undifferentiated cardiac precursors lie medio-dorsally in direct contact with the endoderm in areas where endocardial cells are not detected (***Figure 2A', A''***). This is confirmed by the absence of the endothelial marker CD31 (***Figure 2—figure supplement 2***). We then rendered in 3D the *Nkx2.5^{cre}*-labeled lineages, including both FHF and SHF, and the cTnnT +tissues, including only the FHF/cc, which allowed visualizing the boundary between SHF and cc at the tissue level (***Figure 2A,B,B'***, ***Figure 2—figure supplement 1***, ***Video 3*** and see Materials and methods – non-cardiac tdtomato signal was removed manually).

To identify the changes associated to cardiomyocyte differentiation at the cellular level, we labeled single cells with membrane-GFP (see Materials and methods). cTnnT- progenitors have an epithelial-like columnar cell shape, while the differentiated cTnnT+ cardiomyocytes are rounder and have lost the columnar epithelial organization (***Figure 2C–E*** and ***Figure 2—source data 1***). This is reminiscent of the cell shape transition observed in the distal outflow tract (OFT) at later stages of heart development, when SHF progenitor-to-cardiomyocyte differentiation takes place (***Francou et al., 2014***; ***Ramsbottom et al., 2014***; ***Sinha et al., 2012***). Interestingly, some cells at the boundary zone exhibit weak cTnnT localization and yet show columnar shapes typical of mesodermal cardiac precursors (***Figure 2F–F''''*** and red arrows in ***Figure 2F''', F''''***). Unlike differentiated cardiomyocytes, these cells do not show rounded shapes, and therefore they may represent a transient state between progenitors and differentiated cardiomyocytes; however, the nature of such state cannot be addressed by static analysis. Differentiation of cardiac progenitors is thus accompanied by changes in cell shape and detachment from the endoderm.

We next assessed the expression pattern of the *Nkx2.5eGFP* enhancer reporter line, in which GFP expression is restricted to cardiomyocytes (***Lien et al., 1999***; ***Prall et al., 2007***; ***Wu et al., 2006***). To characterize this reporter line in detail, we immunostained *Nkx2.5eGFP* embryos against cTnnT, ( )(***Figure 3A,B*** and ***Figure 3—figure supplement 1A,B***) and compared the relative intensities of cTnnT and GFP in manually segmented single cells (***Figure 3C,D*** ***Figure 3—figure supplement 2A*** and

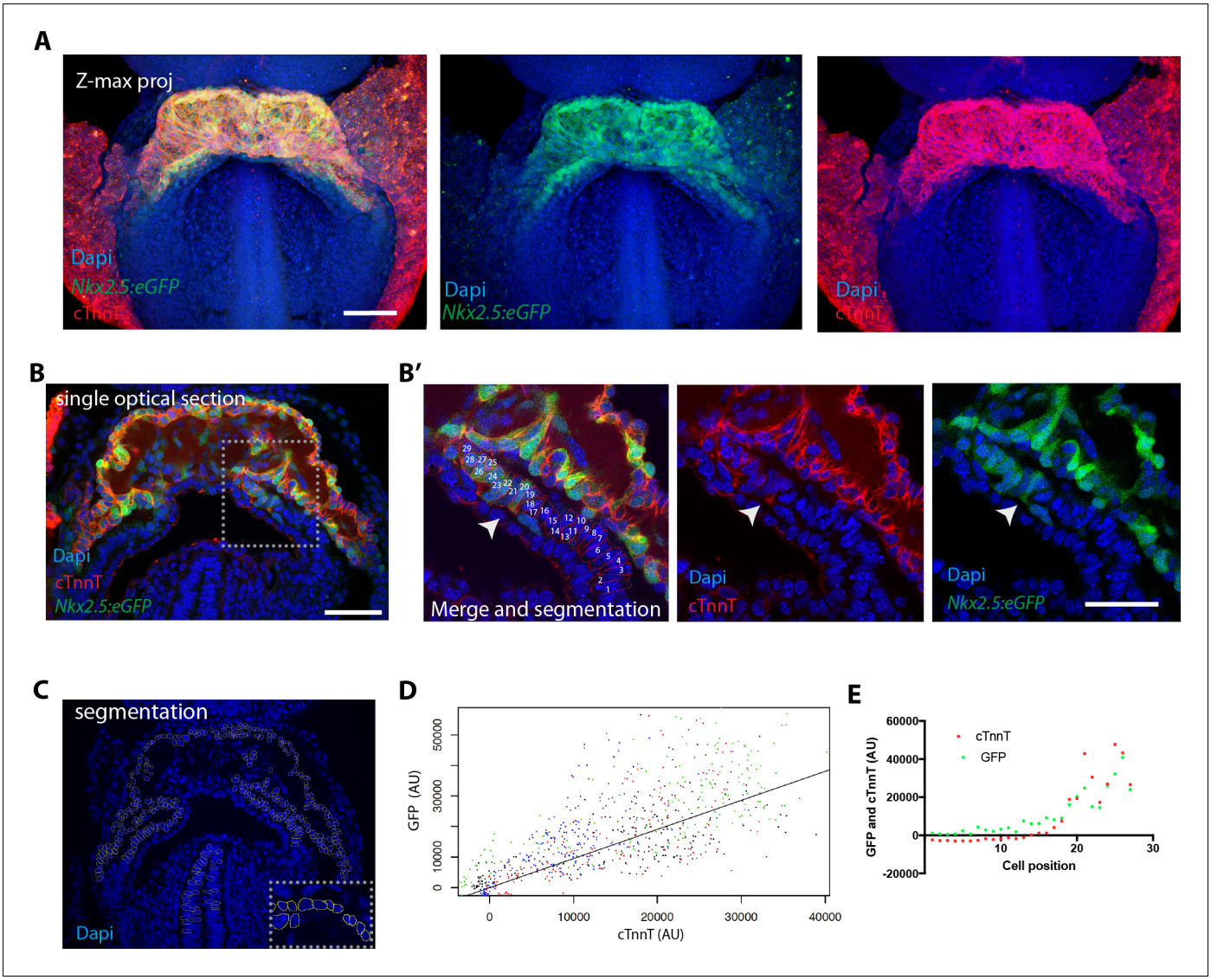

Figure 3. The *Nkx2.5eGFP* transgene is robustly expressed in cTnnT-positive cardiomyocytes. (**A**) z-maximum projection of an *Nkx2.5eGFP* embryo at transversal HT stage immunostained for cTnnT (red) and Dapi (blue) showing high GFP level in differentiated cardiomyocytes. (**B**) Single optical section of an *Nkx2.5eGFP* embryo at transversal HT stage immunostained for cTnnT (red) and Dapi (blue). (**B'**) Inset in (**B**): arrow points the transition between cTnnT+ and cTnnT- domains, corresponding to FHF and SHF, respectively. Dotted line represents the linescan measured in (**D**) (**C**) Example of manual segmentation based on Dapi nuclei in cells located in the splanchnic mesoderm and in the neural tube. (**D**) Linear mixed-effects model to find the relationship between the background-substracted GFP and cTnnT levels adjusted by embryo (GFP = 0.95*cTnnT). (**E**) GFP and cTnnT mean intensities measured within manually segmented cells along the boundary from SHF to cTnnT-positive FHF (**B'**) (n = 130 cells analysed in four independent embryos). Scale bar: 100 μm.

DOI: https://doi.org/10.7554/eLife.30668.015

The following source data and figure supplements are available for figure 3:

Source data 1. Source data for ***Figure 3D and E***.

DOI: https://doi.org/10.7554/eLife.30668.019

Figure supplement 1. The *Nkx2.5eGFP* and cTnnT labeling at different z-levels.

DOI: https://doi.org/10.7554/eLife.30668.016

Figure supplement 2. High GFP levels are detected in strongly labeled cTnnT cells.

DOI: https://doi.org/10.7554/eLife.30668.017

Figure supplement 3. *Nkx2.5Cre* genetic tracing labels both the FHF and SHF.

DOI: https://doi.org/10.7554/eLife.30668.018

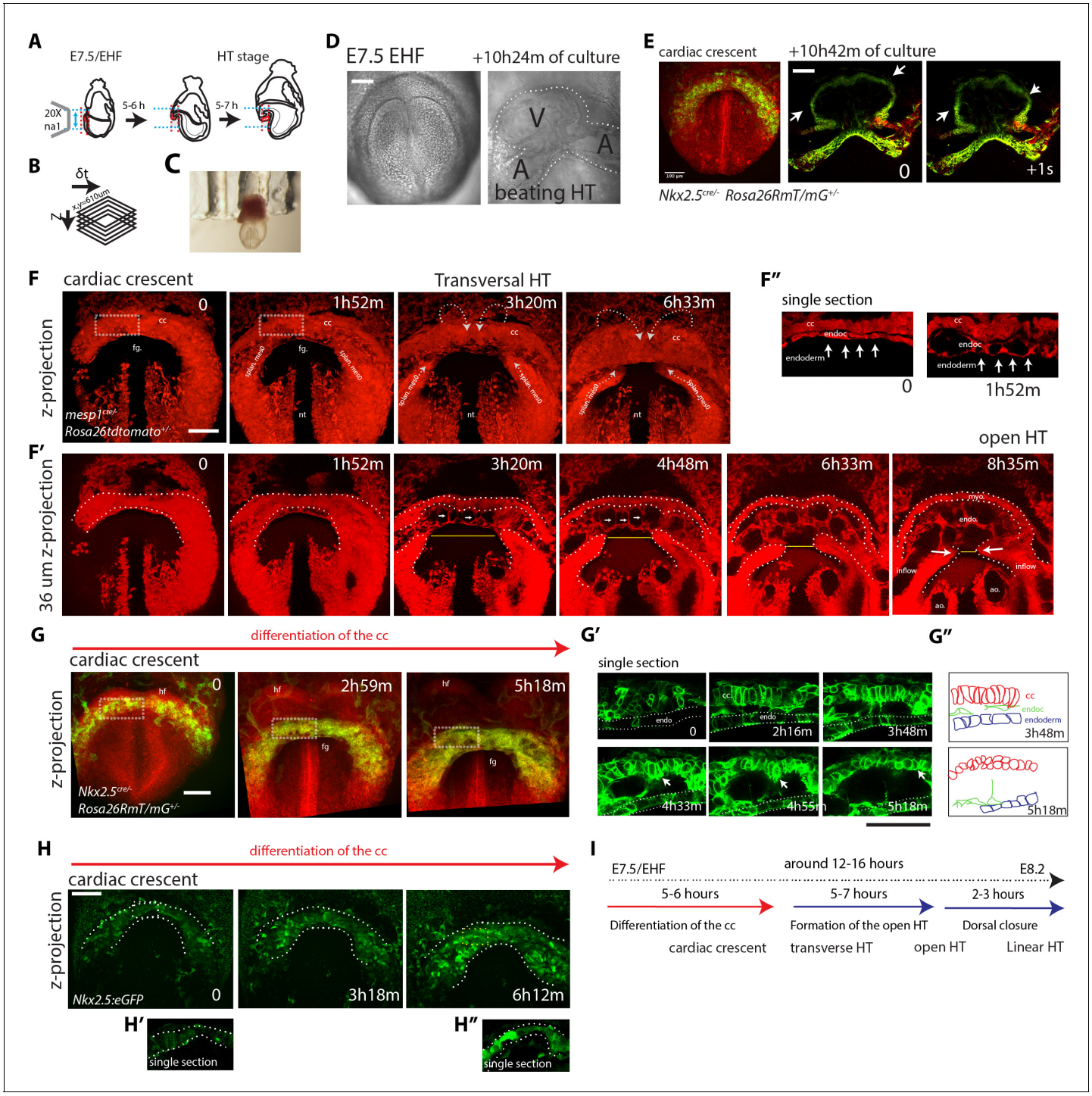

Figure 4. Live-imaging of cardiac differentiation and morphogenesis. (**A**) Schematic of the set up for imaging live mouse embryos from EHF up to completion of HT formation. (**B**) Parameters xyzt during live-imaging. (**C**) An embryonic holder maintains the embryo still during live-imaging. (**D–E**) After over 10 hr of ex-vivo culture inside the two-photon chamber, the embryo has grown and the cardiac crescent has transformed into a beating heart tube. Arrows in (**E**) point to the deformation of the heart ventricle due to heart beats. See also ***Video 4***. (**F–F''**) Time-lapse video sequence of a *Mesp1*$^{cre/+}$; *Rosa26Rtdtomato*$^{+/-}$ embryo –reporting anterior mesoderm–, showing the transition from cardiac crescent stage to heart tube stage. Note that at the initial time point, the foregut pocket is already visible. Arrows indicate the major tissue movements visible (folding of the cardiac crescent, medial movement of the splanchnic mesoderm). The differentiation of cardiomyocytes detaching from the endoderm is visible in (**F'**). White arrows point to the endocardium. The formation of the endocardial lumen in the transversal HT is visible in F'. By 8h35m, the open HT is fully formed and beating regularly. Yellow lines represent distances between the left and right splanchnic mesoderm. Images are z-max projection of 84 sections covering 180 µm (**F**) and 9 sections covering 36 µm (**F'**) acquired every 4 µm. See also ***Videos 5–6***. (**G–G''**) Time-lapse video of an *Nkx2.5*$^{cre/+}$;

Figure 4 continued on next page

Figure 4 continued

Rosa26RmT/mG$^{+/-}$ embryo during the early stages of cardiac differentiation. Images are z-max projection of 87 sections acquired every 5 µm covering 437 µm. (**G'**) shows in a single optical section how progenitors change in cell shape and move away from the endoderm during differentiation toward cardiomyocytes (from inset in (**G**)). (**G''**) Cartoon depicting the change in cell shape taking place during cardiac differentiation. See also ***Video 7***. (**H**) Time-lapse video sequences of *Nkx2.5eGFP* embryos from transversal HT showing low GFP level prior to cardiomyocyte differentiation and increase in GFP intensity level during the stages cardiomyocytes undergo differentiation. (**H' and H''**), cardiomyocytes in single magnified optical sections. Images are z-maximum projections of 70 sections acquired every 6 µm covering 420 µm. See also ***Video 10***. (**I**) Estimate of the timing between different heart tube development stages. fg: foregut cc: cardiac crescent, endoc: endocardium, ao: aorta, endo: endoderm. Scale bars: 100 µm.

DOI: https://doi.org/10.7554/eLife.30668.020

The following source data and figure supplements are available for figure 4:

Source data 1. Source data for Figure ***Figure 4—figure supplement 2***.

DOI: https://doi.org/10.7554/eLife.30668.023

Figure supplement 1. Embryos can be cultured and imaged under the two-photon microscope for up to 24 hr.

DOI: https://doi.org/10.7554/eLife.30668.021

Figure supplement 2. Quantification of the displacement of the splanchnic mesoderm during HT formation.

DOI: https://doi.org/10.7554/eLife.30668.022

Figure 3—source data 1). We found that the GFP level varied linearly with cTnnT level (***Figure 3D***), although considerable variability of GPF levels was observed within each cTnnT+ and cTnnT- cell populations. Scoring of a large number of cells allowed to reproducibly identify the top 50% GFP-expressing cells as positive for cTnnT+ (***Figure 3—source data 1***). Genetic tracing experiments using the *Nkx2.5*$^{cre/+}$*;Rosa26Rtdtomato*$^{+/-}$ line, instead show strong tdtomato level in both the FHF and SHF (***Figure 3—figure supplement 3A***).

We next characterized the boundary between cardiomyocytes and cardiac precursors in transversal HT stage embryos of the *Nkx2.5eGFP* reporter line. We measured mean fluorescent intensity in manually segmented cells at the boundary zone and found that GFP level and cTnnT signals correlate at the individual-cell level (***Figure 3B', E***, ***Figure 3—figure supplement 2B,C*** and ***Figure 3—source data 1***). Altogether, these results indicate that the *Nkx2.5-eGFP* reporter is suitable for tracking cardiomyocytes in live-imaging and reliably identifies the top 50% GFP-expressing cells as cTnnT-positive.

Two-photon live-imaging of early cardiac development in the mouse embryo reveals morphogenetic events leading to HT formation

We next established a live-imaging method to dynamically characterize the formation of the HT in the mouse embryo (***Figure 4A***) (***Chen et al., 2014***). We adapted a previously reported culture system (***Nonaka, 2009***; ***Nonaka et al., 2002***) in which the whole mouse embryo is immobilized by inserting the extraembryonic region in a holder (***Figure 4C***). After culture, embryos showed normal morphology, their hearts were beating and circulation was initiated (***Figure 4D, E*** and ***Video 4***). This culture system in combination with two-photon microscopy enabled the generation of high-resolution 3D+t videos (***Figure 4B*** and see Materials and methods). Maximum culture time and imaging achieved was 24 hr (***Figure 4—figure supplement 1A***, n = 3). However, typical acquisition times varied in most cases between 3 and 13 hr. The rate of acquisition varied in most cases between 4 and 9 min,

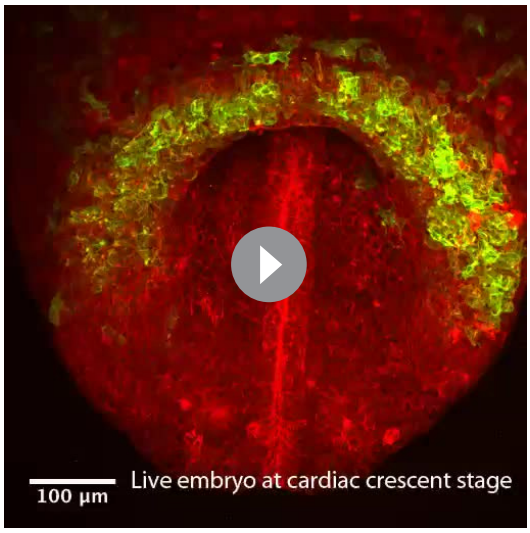

Video 4. z-maximum projection of an *Nkx2.5*$^{cre/+}$*; Rosa26RmT/mG*$^{+/-}$ embryo at cc stage and single-section time-lapse video of the same embryo after 10 hr 42 m of ex-vivo culture (representative analysis from three embryos). Interval between frames: 1 s. Related to ***Figure 4E***.

DOI: https://doi.org/10.7554/eLife.30668.024

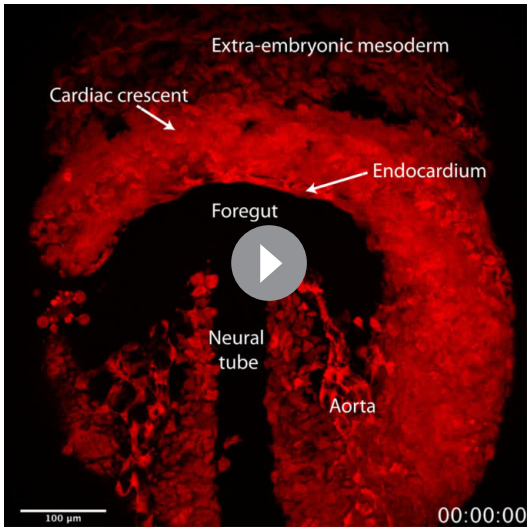

Video 5. Time-lapse video of a *Mesp1*$^{cre/+}$; *Rosa26Rtdtomato*$^{+/-}$ embryo from cc up to open HT stage (h:mm:ss) (representative analysis from four embryos). Interval between frames: 4 m 30 s. Duration of the video: 13 hr 16 m 30 s. Related to ***Figure 4F***.
DOI: https://doi.org/10.7554/eLife.30668.025

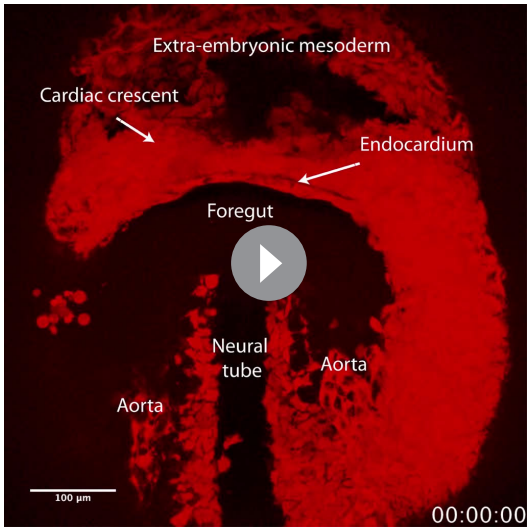

Video 6. Same embryo as in ***Video 5***. Images are z-maximum projection of nine sections acquired every 4 µm covering 36 µm (h:mm:ss) and allows visualization of the inside of the cardiac lumen during HT formation. Interval between frames: 4 m 30 s. Duration of the video: 8 hr 10 m. Related to ***Figure 4F'***.
DOI: https://doi.org/10.7554/eLife.30668.026

with some exceptions depending on the specific aim of the recording (see video legends).

Imaging *Mesp1*$^{cre/+}$; *Rosa26Rtdtomato*$^{+/-}$ embryos allowed tracking the anterior mesoderm (***Saga et al., 1996***; ***Saga et al., 1999***), including cardiac lineages, from cc stage up to HT stage (***Figure 4F,F'*** and ***Videos 5–6***). The time-lapse analysis provided insight on the formation of the endocardial lumen (***Figure 4F', F''***). The endocardium is initially observed as a bilayer of cells and eventually splits into dorsal and ventral layers, which move apart from each other allowing the lumen to become visible between the layers (see ***Videos 6*** and ***7*** for confocal views and ***Video 8*** for a bright field view). Thin cytoplasmic bridges between the endocardial layers persist and extend as the endocardial layers separate from each other (see white arrows in ***Figure 4F'*** and ***Video 6***). Heartbeat becomes detectable around this stage and circulation in the embryo is then initiated.

Imaging *Nkx2.5*$^{cre/+}$; *Rosa26RmT/mG*$^{+/-}$ embryos, in which Cre-recombined cells activate membrane-bound GFP, we could track cells during differentiation, as they transit from a columnar to a round shape and start contracting (***Figure 4G–G''***, ***Video 7*** and bright-field ***Video 8***). We found that the endocardial lumen started to appear while cc cells still remained columnar (compare time points 2 hr 13 m and 3 hr 48 m in ***Figure 4G'***). Cell rounding is therefore unlikely to initiate the formation of the cardiovascular lumen.

Interestingly, this analysis also showed that the transformation of the cc into the HT involves the antero-medial displacement of the splanchnic mesoderm (white arrows in ***Figure 4F,F'***). This displacement promotes the folding of the cardiac

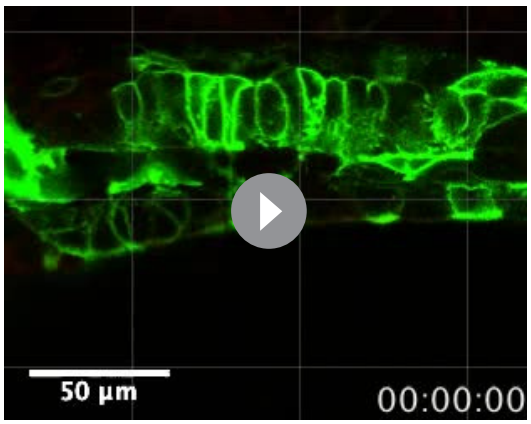

Video 7. Time-lapse video of an *Nkx2.5*$^{cre/+}$; *Rosa26RmT/mG*$^{+/-}$ embryo (h:mm:ss) (representative analysis from two embryos). Interval between frames: 22 m. Duration of the video: 4 hr 02 m. Related to ***Figure 4G–G'***.
DOI: https://doi.org/10.7554/eLife.30668.027

Video 8. Brightfield time-lapse video of a wild type embryo, from cc stage showing the onset of cardiomyocyte contractility and the formation of the cardiac lumen (h:mm:ss) (representative analysis from two embryos). Interval between frames: 1 m 03 s. Duration of the video: 6 hr 04 m 21 s. Representative analysis from two embryos.
DOI: https://doi.org/10.7554/eLife.30668.028

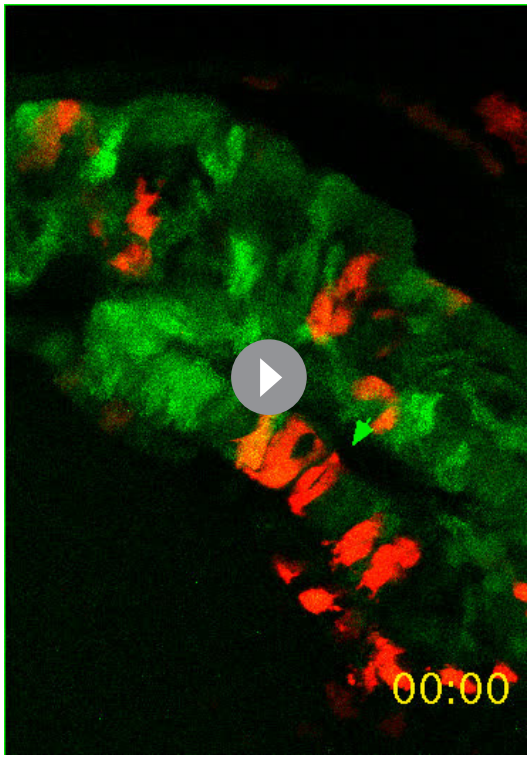

Video 9. Same embryo shown in ***Video 14*** zoomed-in at the level of the splanchnic mesoderm (mm:ss). SHF cells (green arrows) displace antero-medially relative to the underlying endoderm (red arrow). In addition, SHF cells move apart from each other (distance between the green arrows increase from 61 to 83 µm over 3h12m). Related to ***Figure 6H***.
DOI: https://doi.org/10.7554/eLife.30668.029

crescent into a hemi-tube by bringing closer the future borders between the HT and the mesocardium (see yellow lines in ***Figure 4F'*** indicating the distance between the borders at different times). These borders coincide with the frontiers between cardiomyocytes and undifferentiated splanchnic mesoderm (see details in Videos 7, 17 and Figure 7A', A''). Interestingly, the movement of the splanchnic mesoderm is not coherent with the endoderm but a relative displacement is detected between the two layers (***Video 9***). Estimation of splanchnic mesoderm displacement speed toward the midline from time-lapse analyses (***Figure 4F'***, and ***Video 6***) indicates a range of average speeds from 12 to 20 µm/hr (15.8 ± 2.4 µm/hr, mean ±SD, n = 3, ***Figure 4—figure supplement 2*** and ***Figure 4—source data 1***). These measurements estimate that midline convergence of the splanchnic mesoderm takes approximately 5–7 hr from the late cc stage until the open HT stage (***Figure 4—figure supplement 2***).

Our results show the feasibility of live time-lapse analysis of mouse HT formation and reveal that splanchnic mesoderm displacement, at least in part by sliding over the endoderm, is an essential aspect of HT morphogenesis.

Live tracking of cardiomyocyte differentiation in individual cells reveals cardiac crescent differentiation dynamics

Next, to specifically track cardiac differentiation, we used the *Nkx2.5eGFP* live reporter. We first studied the general activation pattern of this reporter in live analysis. At E7/bud stage, a faint and scattered GFP signal is detected in proximity to the yolk sack, at the anterior border of the embryo (***Figure 5—figure supplement 1A***). At neural plate stage, just prior to the ventral folding of the embryo, the GFP signal remains weak but spreads to delineate a crescent in the anterior region of the embryo (***Figure 5—figure supplement 1A*** and ***Video 10***). During about 5–6 hr starting at the EHF stage, the GFP signal increases in intensity, which correlates with the previous observations on cTnnT activation (***Figure 4H***, ***Figure 1C*** and ***Video 11***). From transversal to open HT (5–7 hr) and from the open HT to HT (2–3 hr) the GFP signal remains stable (***Figure 5—figure supplement 1B,B', C,C'*** and ***Video 12***). We conclude that an increase in GFP level in *Nkx2.5eGFP* embryos reports

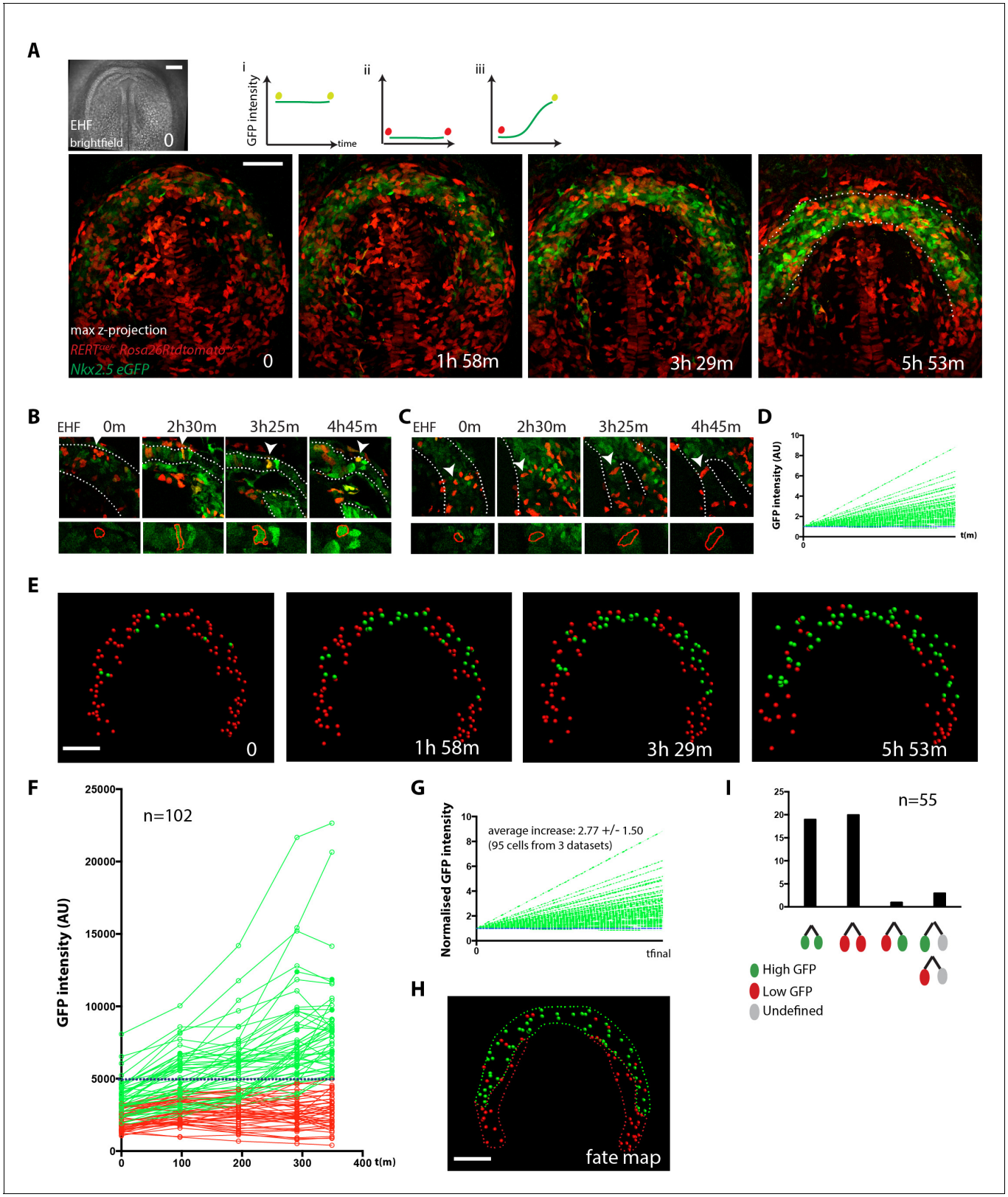

Figure 5. Live-imaging of cardiac differentiation at cellular resolution. (**A**) Time course of an *Nkx2.5eGFP; RERT*$^{cre/+}$*; Rosa26Rtdtomato*$^{+/-}$ embryo during stages when cc differentiation takes place -from EHF onwards-. Images are z-maximum projection of 76 sections acquired every 3 µm covering 228 µm. A bright-field image of the EHF embryo at the initial time point is also shown. (i, ii and iii) Rationale of the expected evolution of GFP expression: since tracks carry information on reporter expression, if a cell acquires a high level of GFP, we predict that it is committed to differentiate.

Figure 5 continued on next page

Figure 5 continued

See also ***Video 12***. (**B–D**) Examples of time-lapse videos (**B and C**) and quantification of the GFP level (**D**) increasing in a single cell during differentiation (**B**) or remaining low in a cell located in the splanchnic mesoderm (**C**). A neural tube cell was additionally quantified (blue). Images are single optical sections. (**E**) Time course of individual cells tracked in the video shown in A. Cells with GFP levels above the median intensity value of all cells at the end of the recording are represented as green spheres and cells with lower GFP levels are shown as red spheres. (**F**) GFP level through time. Blue dotted line: median value (5249 a.u.). GFP level for each tracked cell was measured at five successive time points. Cell divisions are not represented for simplicity. (**G**) Normalized GFP level showing the relative increase in GFP levels for the GFP-positive cells at the end of the recording. Average increase: 2.77 fold ±1.50, mean ±SD, n = 95 cells from three independent videos. (**H**) The position of cells that differentiate (green) and cells that do not is shown in the cc at the initial time point (EHF stage). (**I**) The lineage from cardiac precursors share differentiation fate. Lineages of dividing progenitors (n = 55 from three independent videos) were identified during early stages of cardiac differentiation. Two daughter cells are defined as sharing the same fate if their GFP intensity levels do not differ by more than 1.5-fold and/or both show levels above or below the threshold value defined. Scale bars: 100 μm.

DOI: https://doi.org/10.7554/eLife.30668.033

The following source data and figure supplements are available for figure 5:

Source data 1. Source data for ***Figure 5A,D,F,G,I*** and ***Figure 5—figure supplement 1C,D***.

DOI: https://doi.org/10.7554/eLife.30668.037

Figure supplement 1. Live-imaging of *Nkx2.5eGFP* reporter line.

DOI: https://doi.org/10.7554/eLife.30668.034

Figure supplement 2. Endocardial cells show an elongated shape.

DOI: https://doi.org/10.7554/eLife.30668.035

Figure supplement 3. Cells divide during cardiac differentiation.

DOI: https://doi.org/10.7554/eLife.30668.036

cardiomyocyte differentiation. In addition, these results reveal the timing of the main phases of linear HT development; cc differentiation, formation of the open HT and dorsal closure (***Figure 4I***).

We next sought to track the trajectories and differentiation of individual cardiac precursors within the entire cardiogenic region by 3D+t live imaging. To this end, we used the *Polr2a*^{CreERT2} (*RERT*) allele (***Guerra et al., 2003***), which provides ubiquitous tamoxifen-inducible Cre activity in combination with a *Rosa26Rtdtomato* reporter. We then titrated the tamoxifen dose for a labeling density that would allow single cell tracking during prolonged time-lapse analysis and combined this with the *Nkx2.5eGFP* reporter (see materials and methods). Typically, for each video, we acquired z-slices every 3–5 μm achieving a total z-depth of 200 μm – with some variations depending on the stage considered- and manually tracked in 3D+t for

Video 10. Time-lapse video sequences of *Nkx2.5eGFP* embryos from Early Bud/E7.5 stage (h:mm:ss). (representative analysis from two embryos). Interval between frames: 12 m. Duration of the video: 7 hr 24 m Related to ***Figure 5—figure supplement 1A***.

DOI: https://doi.org/10.7554/eLife.30668.030

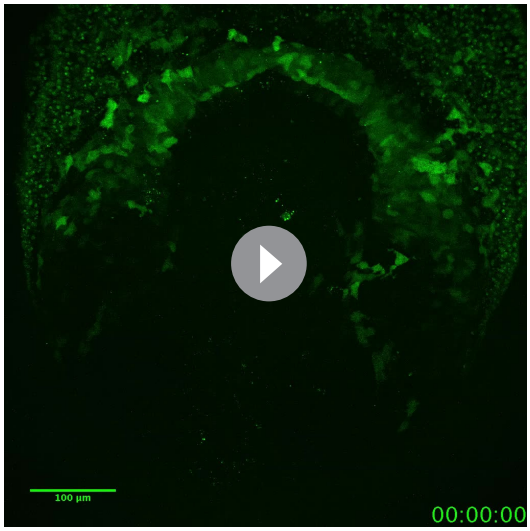

Video 11. Time-lapse video sequences of *Nkx2.5eGFP* embryos from cc to transversal HT stage (h:mm:ss). (representative analysis from three embryos). Interval between frames: 24 m. Duration of the video: 6 hr 48 m. Related to ***Figure 4H***.

DOI: https://doi.org/10.7554/eLife.30668.031

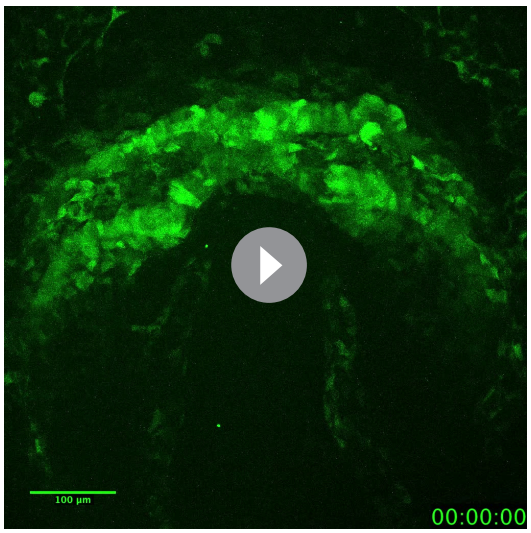

Video 12. Time-lapse video sequences of *Nkx2.5eGFP* embryos from transversal HT to open HT stage (h:mm:ss) (representative analysis from three embryos). Interval between frames: 8 m 09 s. Duration of the video: 5 hr 01 m 33 s. Related to ***Figure 5—figure supplement 1B***.
DOI: https://doi.org/10.7554/eLife.30668.032

several hours an initial population of ~50 to ~100 cells per video, which represents around 5–10% of the total number of cells present in the cc (***de Boer et al., 2012***).

We first tracked cells of the cardiac forming region starting at EHF stage – when cardiac precursors are undifferentiated – up to stages in which cardiomyocytes have differentiated in the cc but the transversal HT stage has not been reached yet (***Figure 5A*** and ***Figure 5—source data 1***). At the onset of cardiac differentiation, the cardiac crescent swings ventrally concomitant with foregut pocket formation. During this movement, we found that the relative positions of the cardiac progenitors are maintained from the initial stage through the differentiated cc (***Video 13***). Relative cell positions therefore remain mostly coherent as the embryonic tissues undergo this initial global movement. Differentiation events are detected in some of the tracked cells by cell shape change from columnar to rounded and by the increase in GFP signal (see example in ***Figure 5B,D*** and ***Figure 5—source data 1***). In contrast, other tracked cells located in the splanchnic mesoderm remain in contact with the endoderm, retain a columnar shape and show low GFP level throughout the videos (***Figure 5C***). These cells are likely to be SHF cardiac progenitors and not endocardial cells, which are not present in this area (***Figure 2—figure supplement 2A,B,B'***). Endocardial cells are instead present in the cardiac crescent and have typical elongated spindle-like shapes (***Figure 4F*** and ***Figure 5—figure supplement 2A***).

Next, in order to establish a fate map of the cardiac forming region at the EHF stage, we tracked back in time the population of cells that showed high GFP intensity (top 50%) at the end of the video (***Figure 5F,H*** and ***Figure 5—source data 1***). According to our previous analysis (***Figure 3D***), these cells can reliably be assigned to cardiomyocytes. The initial location of this cell population fated to become cc cardiomyocytes delineates a crescent-shaped domain at EHF stage (***Figure 5H***). Cells retaining lower GFP intensity level throughout the video initially localize posteriorly and medially to this crescent. Most of the cells that have high GFP levels at the final time point show low GFP levels at the initial time point and increase their GFP level over time (***Figure 5E–G*** and ***Figure 5—source data 1***). These results suggest that cardiomyocytes of the cc differentiate during 5–6 hr starting at the EHF stage, which is consistent with the onset of detectable cTnnT at that stage (***Figure 1B*** and ***Figure 1—figure supplement 3***).

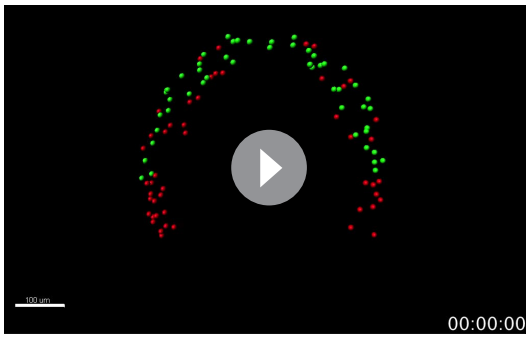

Video 13. Cell tracks in 3D+t during stages when cc differentiation takes place -from EHF onwards- (h:mm:ss). Cells are represented as green spheres if considered GFP+ at the end of the time-lapse analysis and as red spheres when considered GFP- (representative analysis from three embryos). Interval between frames: 19 m 18 s Duration of the video: 5 hr 28 m 06 s. Related to ***Figure 5A***.
DOI: https://doi.org/10.7554/eLife.30668.038

Cells in the cardiac mesoderm do divide during the observation time, so we identified cell division events and tracked the descendant cells. 43% of the tracked cells underwent one division during the 4–5 hr videos. To determine whether cell fate (differentiation versus progenitor) is

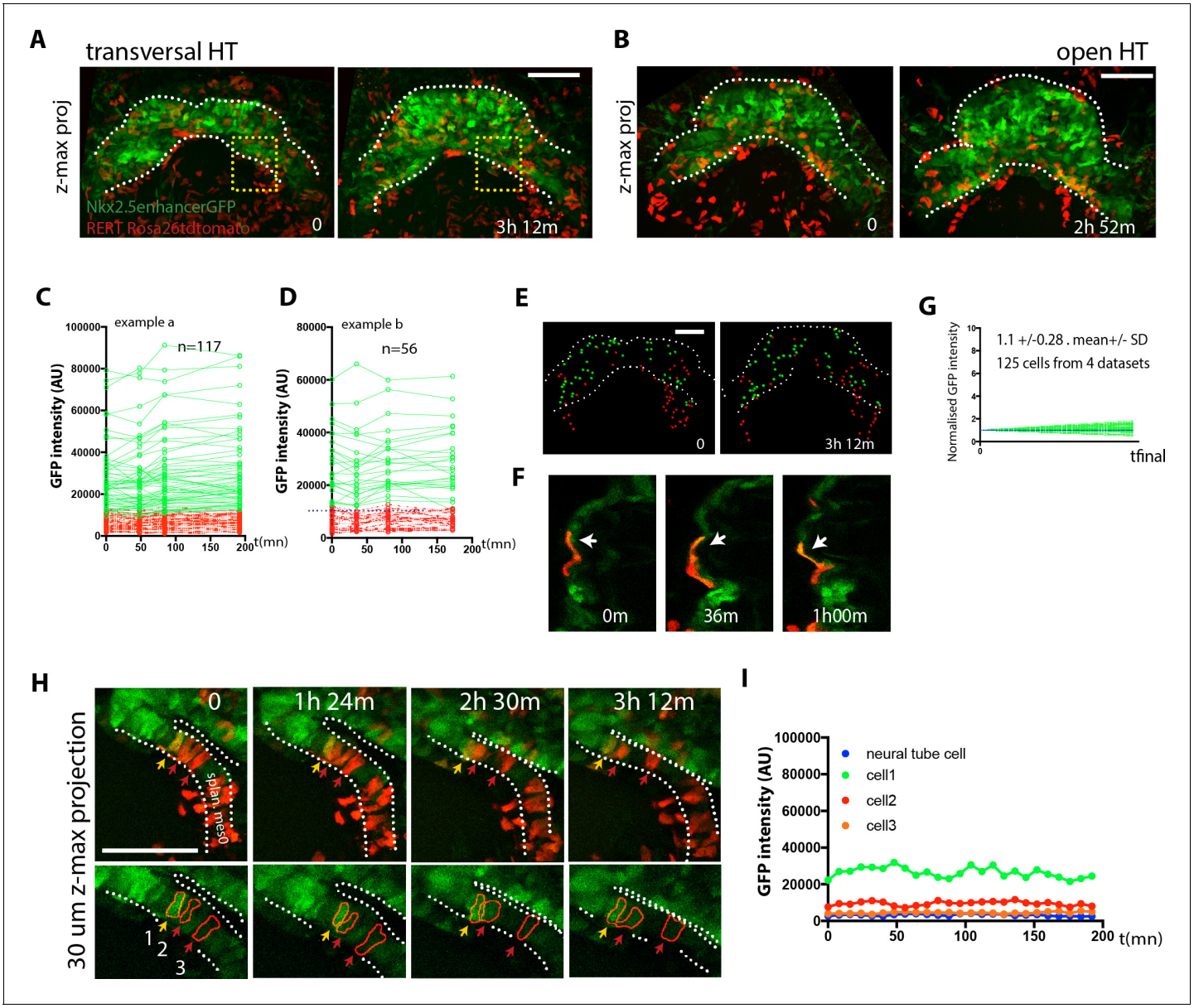

Figure 6. No cardiac differentiation is detected during early HT morphogenesis. (**A–B**) Initial and final time points of two time-lapse videos of tamoxifen-induced *Nkx2.5eGFP; RERT*$^{+/-}$*; Rosa26Rtdtomato*$^{+/-}$ embryos covering the transformation of the transversal HT into the open HT. Images are z-maximum projections of 44 sections acquired every 5 µm covering 220 µm in (**A**) and of 46 sections acquired every 6 µm covering 276 µm in (**B**). See also ***Video 13***. (**C, D**) GFP levels over time of the cells tracked in (**A, B**). GFP level for each tracked cell was measured at four successive time points. Green tracks represent cardiomyocytes with GFP intensity above the median intensity value of all the tracked cells at the last time point, while red tracks represent cells with lower GFP level. Blue dotted line represents the median intensity value (10748 a.u. in (**C**) and 12248a.u. in (**D**)). Note that when cells divide, only one of the two daughter cells was represented for simplicity. (**E**) Distribution of the tracked cells from the time-lapse video shown in (**A**) at the initial and final times of the tracking period. tdtomato+, GFP- cells are represented by red spheres and tdtomato+, GFP +cells are represented by green spheres. (**F**) Example of tdtomato+ cardiomyocytes tracked in the beating ventricle. (**G**) Normalized progression of GFP level in cells classified as GFP+ showing stable GFP levels. Data collected from 125 tracked cells from four independent videos of 2h52m to 3h12m duration. Average increase: 1.1-fold ±0.28, mean ±SD. (**H**) Magnification extracted from the video in A (yellow inset) of tdtomato+ cells in the boundary zone between the undifferentiated and differentiated cells. (**I**) Quantification of GFP level through time of the three segmented cells shown in (**H**). Cells show stable GFP levels and do not differentiate. Images are z-maximum projections of 6 sections acquired every 5 µm covering 30 µm. Scale bars: 100 µm.

DOI: https://doi.org/10.7554/eLife.30668.039

The following source data and figure supplement are available for figure 6:

Source data 1. Source data for ***Figure 6A,B,C,D,G,I***, ***Figure 6—figure supplement 1A***, ***Figure 6—figure supplement 1B and C***.

DOI: https://doi.org/10.7554/eLife.30668.041

Figure 6 continued on next page

Figure 6 continued

Figure supplement 1. Longer videos can capture both initial cardiac differentiation in the FHF and early HT morphogenesis.
DOI: https://doi.org/10.7554/eLife.30668.040

allocated in the cardiogenic mesoderm at the EHF stage, we tracked GFP levels in dividing cells and their descendants. We found that most sister cell pairs show matched high or low GFP intensity levels at the end of the observation period (38 out of 39, ***Figure 5I***, ***Figure 5—figure supplement 3A–D*** and ***Figure 5—source data 1***). This observation suggests that commitment of cardiac precursors to differentiation is already established by the EHF stage and largely transmitted by lineage.

Cardiomyocyte differentiation is not detected during heart tube morphogenesis

We next studied cardiac differentiation dynamics during subsequent stages when the cc transforms into the HT by extensive morphogenesis. To do so, we tracked cells located in the splanchnic mesoderm and cc in *Nkx2.5-eGFP* embryos at successive periods of around 3 hr covering the 5–7 hr during which the transversal HT transforms into the open HT (***Figure 6A,B,E***, ***Video 14*** and ***Figure 4—source data 1***). This analysis revealed that the trajectories of cc cells move apart from each other over time as the tissue expands during the transition from the transverse HT to the more spherical open HT. The HT starts to beat during the observation period, especially at the later stages, and therefore, in some cases, cardiomyocyte cell shape appears distorted in single optical sections (***Figure 6F***); however, the GFP level could be determined. As mentioned above, antero-medial movement of the splanchnic mesoderm can be observed concomitant with the transformation of the transversal HT into the open HT (visible also in ***Videos 5*** and ***12***). We found that cells with high GFP level at the initial time points –differentiated cardiomyocytes – retain rather stable GFP levels (green tracks in ***Figure 6C,D,G*** and ***Figure 6—source data 1***). In addition, all cells that initially showed low GFP levels did not increase GFP intensity during time-lapse; thus new events of cardiac differentiation were not detectable by this approach (red tracks in ***Figure 6C,D***). Tracking cells for longer periods of time, covering from cc differentiation continuously up to the open HT stage, confirmed that cc differentiation is followed by a period of time in which no differentiation events occur (***Figure 6—figure supplement 1***, n = 19 cells tracked in one embryo).

To confirm the absence of detectable cardiac differentiation events during this period, we next focused on the live analysis of cells located at the boundary between cardiomyocytes and undifferentiated splanchnic mesoderm. As expected, we observed GFP-low cells located adjacent to GFP-high cells in the boundary zone (***Figure 6H*** and ***Video 14***). Those cells retain stable GFP levels throughout the tracking time and did not increase their GFP level (***Figure 6I***, boundary imaged 20 times in different locations and in six independent embryos). Importantly, they retain a columnar shape typical of weak cTnnT+ and cTnnT- cells located at the boundary zone (see ***Figure 2F''*** and ***Figure 3B'***). Although these cells migrate antero-medially relative to the underlying more static endodermal cells (see endodermal cell highlighted by the red arrow from t = 69 m in ***Video 9***), they do not contribute to the HT during the observation period. We confirmed this observation in longer time-lapse videos spanning 7 hr that covered the whole transition from transversal to open HT stage. Again, progenitors strictly respected the boundary with the HT throughout the entire time-lapse video (***Figure 7A–A'''*** and ***Video 15***, boundary imaged five times in different locations and in two independent embryos). All together, these data suggest that during the transformation of the cc into the dorsally open HT no cardiomyocytes are

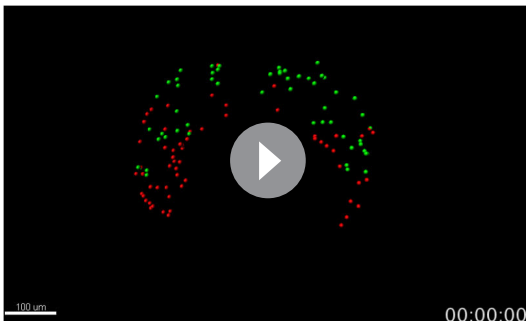

Video 14. Cell tracks in 3D+t during stages the open HT forms. Cells are represented as green spheres if considered GFP+ at the end of the time-lapse analysis and as red spheres when considered GFP- (Representative analysis from three embryos). Interval between frames: 7 m 40 s. Duration of the video: 3 hr 12 m. Related to ***Figure 6A***.
DOI: https://doi.org/10.7554/eLife.30668.042

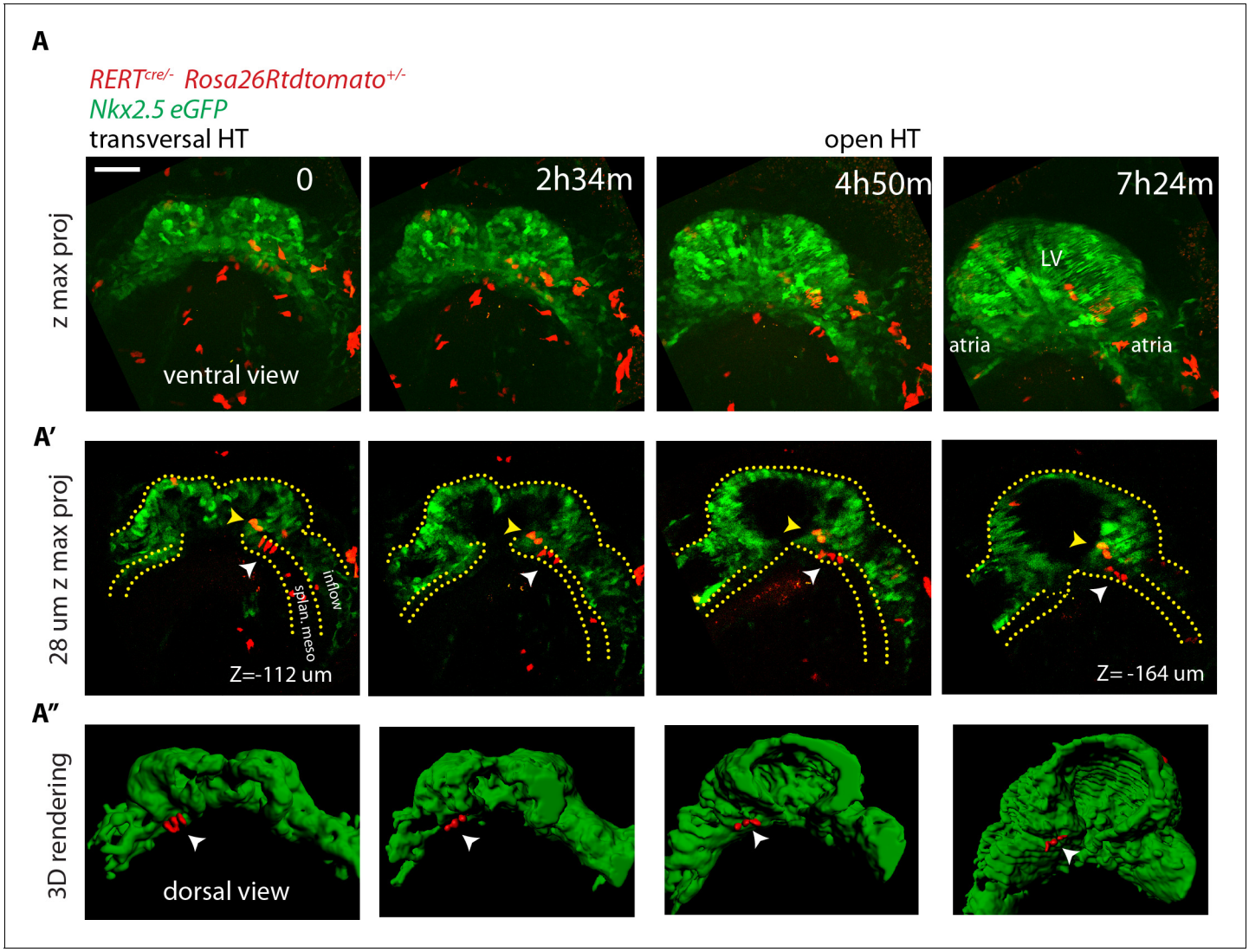

Figure 7. No cardiac differentiation is detected during early HT morphogenesis. (**A–A''**) Images from time-lapse ***Video 15*** of a tamoxifen-induced *RERT*$^{+/-}$*; Rosa26Rtdtomato*$^{+/-}$*; Nkx2.5eGFP* embryo during the stages at which the transversal HT transforms into an open HT, showing cells located in the splanchnic mesoderm (white arrows in A' and A''), respecting the boundary with the HT (yellow arrows in J' show two cells located in the HT). Lower doses of tamoxifen were injected in order to label only a very small proportion of cells in red. Images are z-maximum projection of 74 sections (**A**), acquired every 4 µm covering 296 µm and (**A'**) 7 sections covering 28 µm. (**A''**) 3D reconstruction based of the *Nkx2.5eGFP* signal (green) and tdtomato +cells located in the splanchnic mesoderm. See also ***Video 14***. Scale bars: 100 µm. Splan. meso: splanchnic mesoderm.
DOI: https://doi.org/10.7554/eLife.30668.043

added to the HT from the SHF. These observations suggest two distinct phases of early HT formation: a first phase of differentiation of the FHF into the cc, lasting around 5 hr, and a second phase of HT morphogenesis in which the SHF progenitors remain undifferentiated, lasting around 5–7 hr. During this second phase, extensive remodeling of the cardiac crescent is concomitant with the antero-medial splanchnic mesoderm displacement.

Imaging the Isl1-expressing cell lineage confirms absence of cardiac progenitor differentiation during early heart tube morphogenesis

The LIM domain transcription factor Islet1 (Isl1) is a cardiac progenitor marker. Its expression is transient in the precursors of the cc, while it remains expressed in SHF progenitors for an extended period (***Brade et al., 2007***; ***Prall et al., 2007***; ***Yuan and Schoenwolf, 2000***). Cells of the *Isl1*-expressing lineage detected with Cre reporters therefore contribute only scarcely to the cc, while

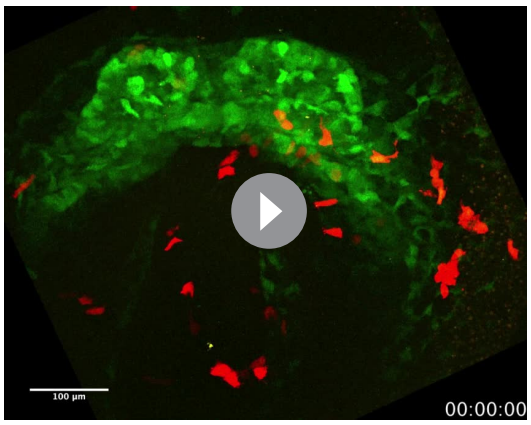

Video 15. Time-lapse video of a *RERT*$^{+/-}$; *Rosa26Rtdtomato*$^{+/-}$; *Nkx2.5eGFP* embryo during the stages at which the transversal HT transforms into the open HT (h:mm:ss). Interval between frames: 19 m 19 s. Duration of the video: 7 hr 24 m 35 s. (2nd half) 3D reconstruction at three time points based of the eGFP signal (green) and red-labeled cells located in the splanchnic mesoderm. Related to ***Figure 7A***.
DOI: https://doi.org/10.7554/eLife.30668.044

extensively to the SHF and its derivatives (***Cai et al., 2003***; ***Ma et al., 2008***). To test these observations in live imaging, we combined *Nkx2.5eGFP* with tracing of the *Isl1* cell lineage using the *Isl1*^{cre} driver and the *Rosa26Rtdtomato* reporter. We found that tdtomato labeling is first detectable in scarce isolated cells of the GFP+ cc during the period when the cc swings ventrally and differentiates (from t = 2 hr 36 m to t = 4 hr in ***Figure 8A,B***). In contrast, a dense tdtomato labeling appears in the GFP-low cells of the splanchnic mesoderm as the cardiac crescent fully differentiates (from t = 2h24 m to t = 4 hr in ***Figure 8A and C*** and ***Video 16***). tdtomato is as well detected in the endoderm and endocardium (not shown). Consistently with previous reports (***Cai et al., 2003***), *Isl1*^{cre}-induced recombination detected in live analysis is thus low in the cc and complete in the SHF.

Once the cc is formed, if cells of the SHF would continuously differentiate, then regions of the forming heart tube contributed by the SHF precursors should appear densely co-labeled with both GFP and tdtomato. Live imaging shows instead that tdtomato+ cells establish a boundary with GFP+ cells, confirming no signs of differentiation of SHF precursors during the observation period (***Figure 8A,C*** and ***Video 17***). The live imaging, however, did not allow to unambiguously identify all cells located deep inside the live tissue at the final stages recorded. The arterial pole in particular is located deep in the embryo. It is therefore challenging to accurately track cardiac differentiation by the increase of GFP levels there (***Figure 8—figure supplement 1A–A''***, from around 200 µm depth, see next section). To overcome these limitations, we fixed and immunostained embryos against cTnnT after completion of the live-imaging experiments, and imaged them by 3D confocal microscopy. No solid domains containing double-labeled cells were detected, indicating that progenitors located in the SHF did not undergo differentiation in the boundary zone from cc to open HT stage (***Figure 8D***). These results are consistent with the single-cell tracking analysis and confirm that the SHF does not differentiate during linear HT morphogenesis.

Cardiac differentiation is detected during the late stages of HT development

We next wanted to determine when cardiac progenitors located in the SHF start to differentiate. In order to address the timing of SHF contribution to the arterial pole, we next fixed and optically cleared *Nkx2.5eGFP; Ils1*$^{cre/+}$; *Rosa26Rtdtomato*$^{+/-}$ embryos at different stages from cc up to heart looping (n = 10) and assessed the appearance of GFP and tdtomato double-positive domains in the HT. In agreement with our previous observations, we found that SHF cells do not differentiate up to the open HT stage, when the dorsal seam of the heart is still open. In contrast, massive appearance of solid domains of double positive cells is observed subsequently in the fully closed HT, reinforcing our previous interpretation (***Figure 9A,B*** and ***Videos 18,19***). At this stage, the primordium of the RV has been added at the arterial pole (***Zaffran et al., 2004***; ***Laugwitz et al., 2005***; ***Moretti et al., 2006***) and is fully composed of double-positive cells. The dorsal seam of the HT is also densely populated by double-positive cells, indicating a contribution of precursors from the splanchnic mesoderm to the cardiomyocyte population that finalizes the dorsal closure of the linear HT.

In order to capture the initiation of SHF contribution to the HT by live imaging, we first focused on the venous pole, as this region is more directly exposed than the rest of the HT and therefore more suitable for live-imaging. In videos that captured the transition from the open HT to the closed linear HT, some cells at the border between the FHF and SHF maintain low GFP levels during the first part of the recording and upregulate GFP to the level of the cardiomyocyte population as the

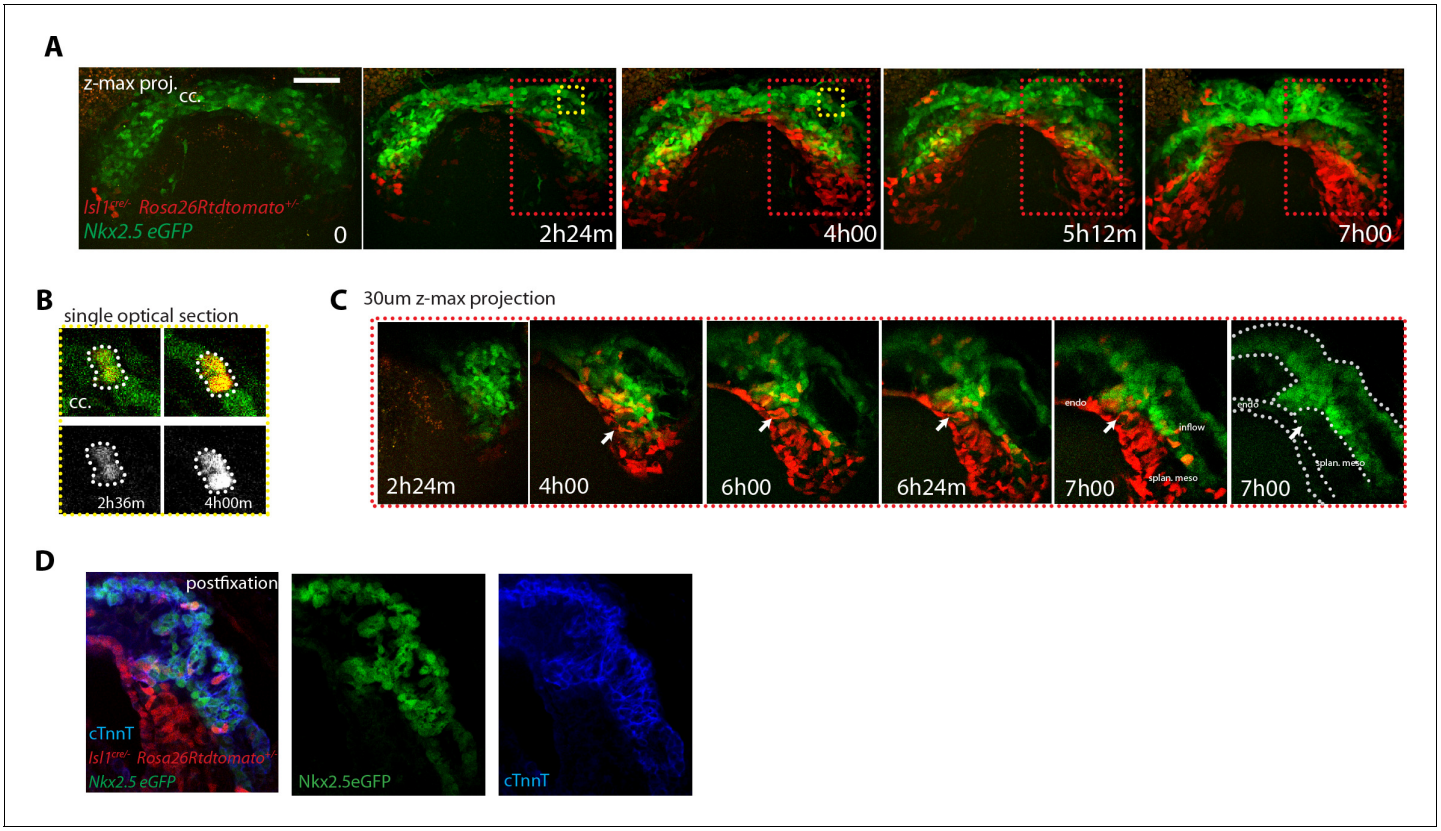

Figure 8. SHF Isl1-expressing cells do not contribute to the early open-heart tube. (**A**) Image sequence from time-lapse ***Video 16*** of an *Isl1$^{cre/+}$; Rosa26Rtdtomato$^{+/-}$; Nkx2.5eGFP* embryo showing that recombination driven by *Islet1^{cre}* of the *Rosa26* locus is complete in the splanchnic mesoderm and scarce in the FHF (n = 3 videos from cc up to open HT stage). (**B**) Inset from A (yellow frame). Two cells of the Isl1+ lineage located in the cc increase their tdtomato level over time. (**C**) Inset from A (Red frame); increase of the tdtomato intensity in the splanchnic mesoderm over time. Arrow shows the boundary between SHF and FHF and points to a single cell in the SHF that retains a low level of GFP and a columnar shape. Note that tdtomato signal is also detectable in the endoderm. Images are z-maximum projection of 45 sections acquired every 5 µm and covering 225 µm in (**A**) and of 6 sections covering 30 µm in (**C**). (**D**) Same embryo as in (**A**) post-fixed and immunostained against cTnnT after live-imaging, showing that the red cells located in the splanchnic mesoderm are undifferentiated. Scale bars: 100 µm.

DOI: https://doi.org/10.7554/eLife.30668.045

The following source data and figure supplements are available for figure 8:

Source data 1. Source data for ***Figure 8—figure supplement 2C***.

DOI: https://doi.org/10.7554/eLife.30668.048

Figure supplement 1. GFP level in deeper z levels cannot be accurately quantified.

DOI: https://doi.org/10.7554/eLife.30668.046

Figure supplement 2. Cells increasing their GPF expression can be detected at the venous pole during activation of SHF contribution to the HT.

DOI: https://doi.org/10.7554/eLife.30668.047

HT forms (***Figure 8—figure supplement 2***). We next aimed to live-track the activation of SHF differentiation at the arterial pole. Because of the imaging limitations in this area, quantitative analysis of the GFP signal was not possible and we instead used the qualitative detection of SHF cells addition to the HT. To achieve this, we imaged an *Nkx2.5eGFP; Ils1$^{cre/+}$; Rosa26Rtdtomato$^{+/-}$* embryo at successive time points throughout the transition from open to linear HT and tracked tdtomato+ cells incorporation to the HT at the arterial pole. This study further confirmed that SHF differentiation at the arterial pole is initiated when the HT is about to close dorsally but not before (***Figure 9C***). Thus, SHF cells do not differentiate during the 5–7 hr period when morphogenesis of the open HT takes place, but coordinately start differentiation at different regions of the HT during dorsal closure. Interestingly, these regions do not only include arterial and venous poles but also the dorsal seam of the HT.

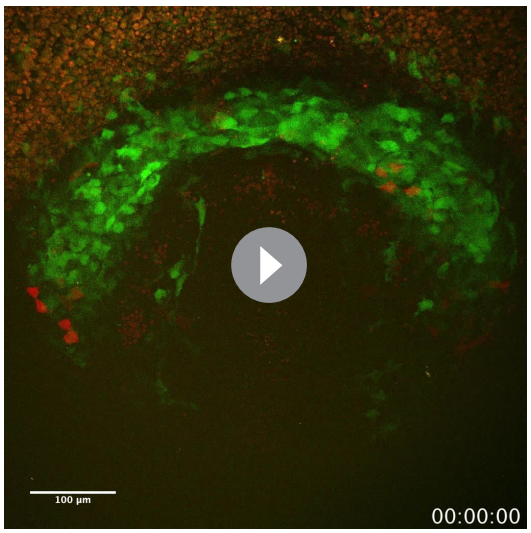

Video 16. Time-lapse video of an *Isl1$^{cre/+}$; Rosa26Rtdtomato$^{+/-}$; Nkx2.5eGFP* embryo (h:mm:ss) (representative analysis from three embryos). Interval between frames: 6 m. Duration of the video: 7 hr 18 m. Related to ***Figure 8A***.
DOI: https://doi.org/10.7554/eLife.30668.049

Discussion

Here, we established a whole-embryo live-imaging method based on two-photon microscopy that allows whole-tissue tracking at cellular resolution. By combining various genetic tracing tools, we labeled progenitor and differentiated cardiomyocytes and performed 3D cell tracking over time combined with 3D reconstruction of the HT at multiple stages. We report three distinct temporal phases of HT formation (***Figure 10***). During the first phase, the cc differentiates rapidly and morphogenesis, in terms of changes in the relative position of cells, is minimal. During the second phase, differentiation is not detected and morphogenetic remodeling gives rise to a dorsally open HT. During the third phase, cardiac precursor recruitment and differentiation resumes, contributing to the formation of the RV and the dorsal closure of the HT. Our results support the early establishment of distinct FHF and SHF cell populations and show that the morphogenetic changes that transform the cc into a HT largely take place in the absence of cardiac precursor differentiation. These observations indicate tissue-level coordination of differentiation and morphogenesis during early cardiogenesis in the mouse.

The series of 3D reconstructions from fixed embryos was important to establish a reference staging of HT formation. This allowed us to accurately stage embryos in live experiments based on morphology and it will also be useful in the future for gene expression mapping and accurate phenotypic analysis of mutant embryos. The tissue growth pattern observed in static 3D reconstructions was insightful to suggest variability in growth rates during different phases of HT formation. Growth of the differentiated cardiac tissue is relatively paused when the cc undergoes morphogenesis to form the open HT during the second phase. This is consistent with previous studies in mouse, chick and human models showing that proliferation drops in the

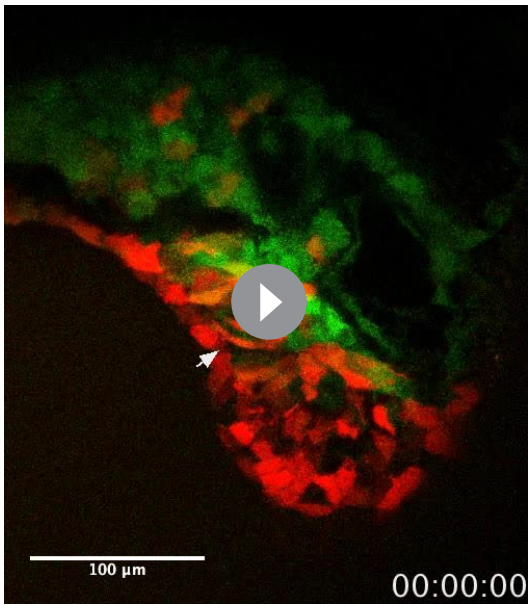

Video 17. Same embryo shown in ***Video 16*** zoomed-in at the level of the splanchnic mesoderm (h:mm:ss). Related to ***Figure 8C***.
DOI: https://doi.org/10.7554/eLife.30668.050

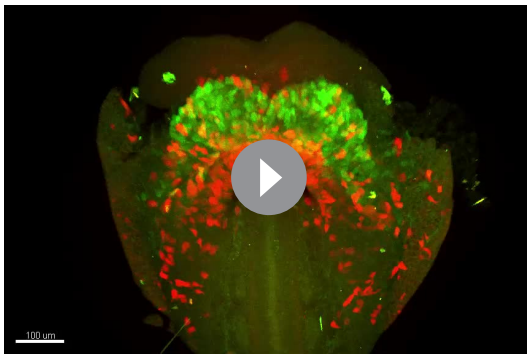

Video 18. 3D rendering of an *Isl1$^{cre/+}$; Rosa26Rtdtomato$^{+/-}$; Nkx2.5eGFP* embryo at transversal HT stage. Related to ***Figure 9A***.
DOI: https://doi.org/10.7554/eLife.30668.052

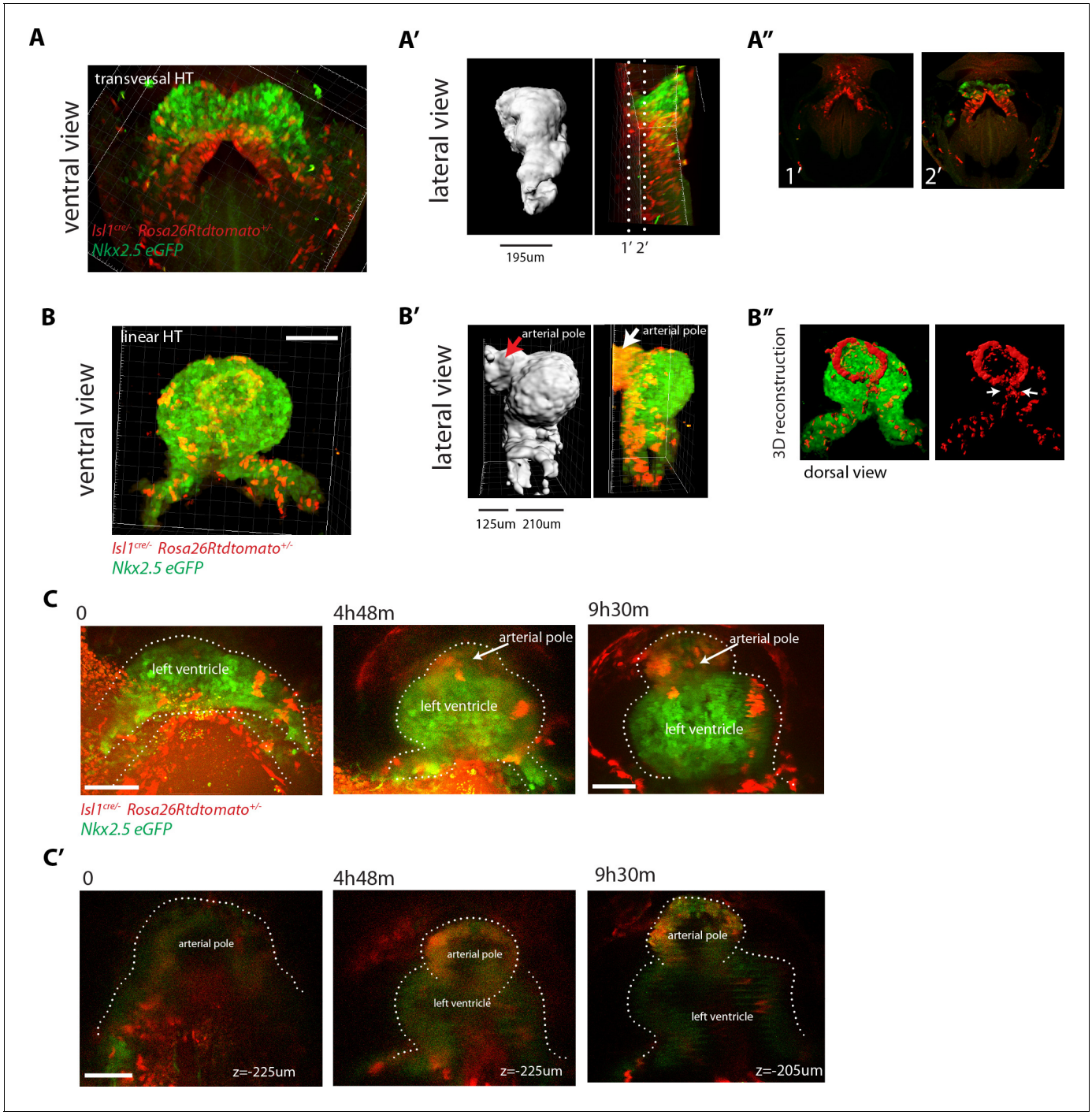

Figure 9. SHF Isl1-expressing cells contribute to the arterial pole during late linear HT morphogenesis. (**A, B**) *Isl1$^{cre/+}$; Rosa26Rtdtomato$^{+/-}$; Nkx2.5eGFP* embryos showing no contribution of the Isl1 lineage to the transversal HT (**A–A''**) but contributing robustly to the arterial pole and dorsal aspect of the linear HT (**B– B''**). The presence of double-positive cells in these areas reveals the differentiation of Isl1 lineage cells into cardiomyocytes (**A, B**). Images are 74 and 134 optical sections acquired every 2.5 µm and covering 195 µm and 335 µm, respectively. In (**B, B'**) only the double-positive cells located in the linear HT are shown, while the tdtomato+ progenitors, located outside the linear HT are not shown. Lateral views are shown in (**A', B'**) including 3D reconstructions. (**A''**) Cross-sections in xy along the dotted lines shown in (**A'**). Dorsal views are shown in (**B''**) including the 3D reconstruction of the tdtomato+ cells located in the linear HT. White arrows show the dorsal (mesocardial) regions of the linear HT. (**C**) Snapshots of an *Ils1$^{cre/+}$; Rosa26Rtdtomato$^{+/-}$; Nkx2.5eGFP* embryo at different time points during the third phase showing that the tdtomato+ SHF cells contribute to the arterial pole of the HT. Images are 52 optical sections acquired every 5 µm and covering 260 µm. The embryo was imaged continuously every 13 m for the first 6 hr of culture and then imaged once again at time point 9h30m. Note that at the last time point, the laser was increased at maximum power in order to reveal more clearly the red labeled cells at the arterial pole. The contrast had to be enhanced as well. (**C'**) Images at time points 0, 4h48m and

Figure 9 continued on next page

Figure 9 continued

9h30m. Images at time points 0 and 4h48m are z-maximum projection of 5 sections covering 25 µm. Image at 9h30m is a single optical section. at: arterial pole. endo: endoderm, splan meso: splanchnic mesoderm. Scale bars: 100 µm.

DOI: https://doi.org/10.7554/eLife.30668.051

differentiated myocardium of the forming HT, while proliferation remains high in the splanchnic mesoderm (***van den Berg et al., 2009***; ***de Boer et al., 2012***; ***Sizarov et al., 2011***). Our live analysis further showed that SHF cells do not contribute to the forming HT during the differentiation pause, which correlates with the growth rate reduction during this phase. This period coincides as well with the onset of cardiac contractility in the embryo (***Tyser et al., 2016***).

Following the phase of differentiation pause, growth of the HT is reinitiated by incorporation of new cells as the HT closes dorsally and the RV precursors are added at the arterial pole during the third phase. During this third phase, similarities were found in the differentiation dynamics of SHF precursors and splanchnic precursors contributing to the dorsal regions of the linear HT. The dorsal aspect of the linear HT gives rise to the inner curvature of the looped heart, which has an important contribution to non-chamber myocardium, including atrio-ventricular canal and parts of the conduction system (***Christoffels et al., 2000***). Our results suggest that the late recruitment of progenitors to the dorsal HT could contribute to differences between inner curvature cardiomyocytes and the rest of the heart tube.

While the live-imaging experiments were essential for the identification of the 5–7 hr hiatus between FHF and SHF differentiation, live imaging of the arterial pole during the SHF differentiation phase was challenging and was complemented by 3D reconstructions based on fixed and optically cleared embryos. These experiments confirmed the pause in differentiation during open HT formation and its reactivation during linear HT closure. In the future, it will be interesting to explore whether novel non-toxic index-matching media compatible with embryo viability (***Boothe et al., 2017***) may alleviate the limitations for deep cardiac imaging during late HT formation.

Regarding the specification of FHF and SHF populations, previous prospective clonal analyses showed that these lineages diverge around gastrulation (***Devine et al., 2014***; ***Lescroart et al., 2014***). In agreement with this, our tracking of cell lineages in the cardiac forming region shows that sister cells share fates to either the cardiac crescent or the SHF. In addition, the fact that cells contributing to the SHF do not differentiate during the period when the cardiac crescent transforms into the primitive heart tube may contribute to the establishment of the sharp boundary observed between left and right ventricles later in development (***Devine et al., 2014***). Further studies will be required to assess how this temporal pause of cardiac differentiation is regulated. The molecular analyses of early FHF and SHF precursors suggest that intrinsic molecular differences between the two lineages appear around or shortly after gastrulation (***Lescroart et al., 2014***). These intrinsic differences may contribute to the regulation of the two distinct differentiation schedules described here. These studies and our observations, however, cannot discriminate whether this lineage allocation results from intrinsic differences between these lineages or it is due to their exposure to position-specific environments, especially as in our studies sister cells remain close neighbors. Environmental cues thus could also control the sequential differentiation of FHF and SHF precursors. The Wnt and BMP pathways are well known regulators of cardiac differentiation (***Ai et al., 2007***; ***Jain et al., 2015***; ***Klaus et al., 2007***; ***Kwon et al., 2007***; ***Marvin et al., 2001***; ***Qyang et al., 2007***; ***Tirosh-Finkel et al., 2010***; ***Ueno et al., 2007***) and specific mechanisms affecting these pathways could be operating during the formation the HT, whereby the differentiation pathways could be temporally restrained. Finally, the endoderm

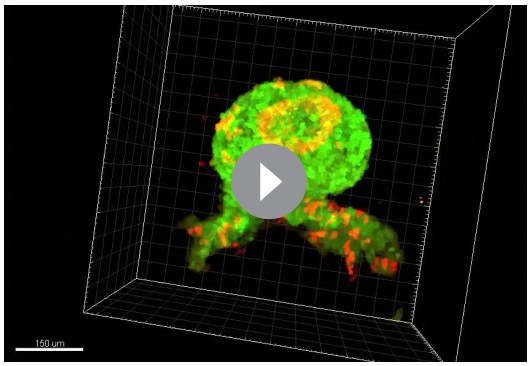

Video 19. 3D rendering of an *Isl1$^{cre/+}$; Rosa26Rtdtomato$^{+/-}$; Nkx2.5eGFP* embryo at linear HT stage. Related to ***Figure 9B***.

DOI: https://doi.org/10.7554/eLife.30668.053

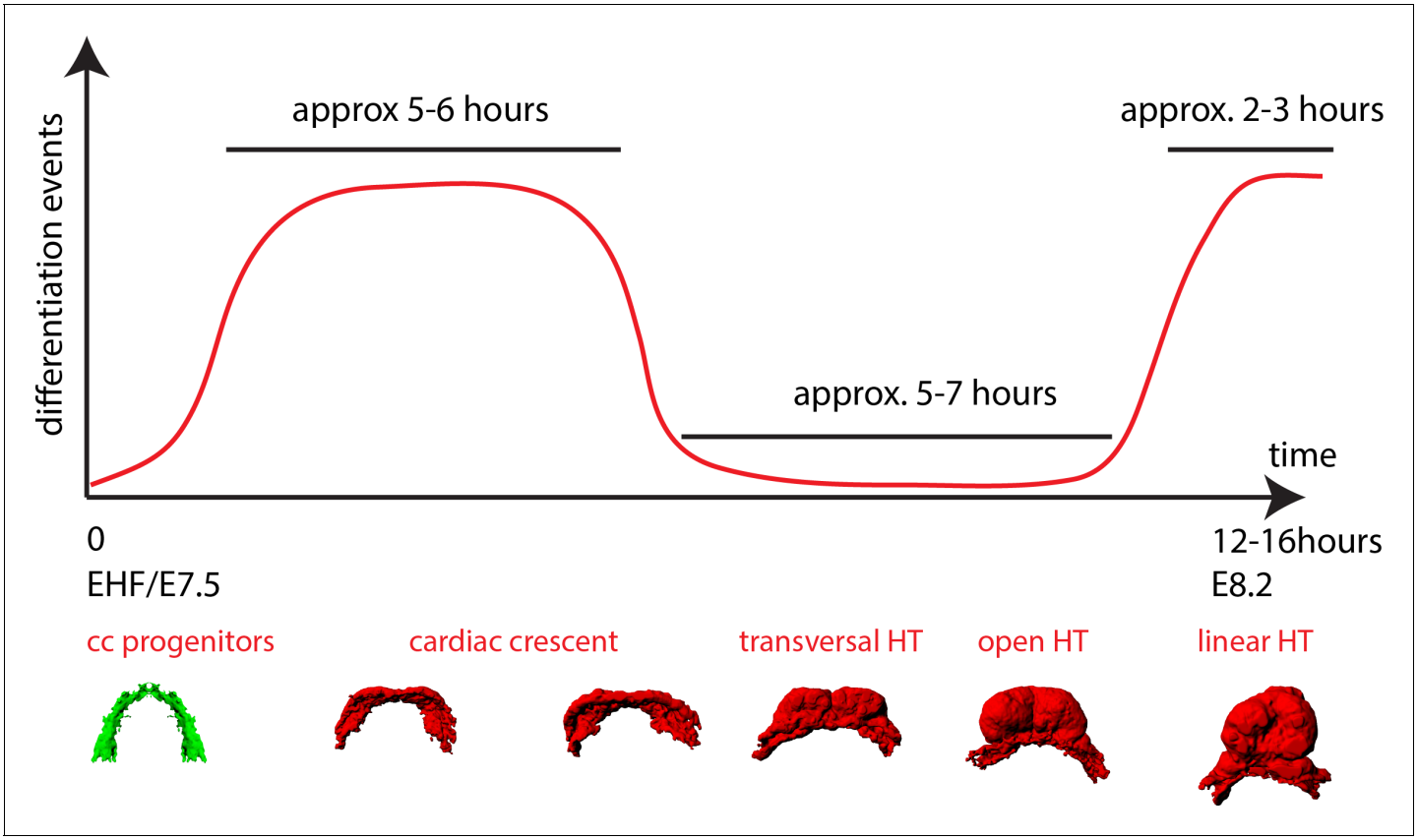

Figure 10. A model of cardiomyocyte differentiation dynamics during early heart development. We propose that two distinct phases of cardiomyocyte differentiation take place during early heart development. At EHF stage the cc differentiates and starts folding. Cardiomyocytes round up and become contractile while the cardiac progenitors located in the splanchnic mesoderm remain undifferentiated. Subsequently, the cc. undergoes further morphogenesis to transform into a HT, initially open dorsally and no cardiomyocyte differentiation is detected during this transformation. Finally, cardiac differentiation resumes contributing new cardiomyocytes from the splanchnic mesoderm to the arterial pole (prospective RV) and the dorsal closure of the HT.

DOI: https://doi.org/10.7554/eLife.30668.054

may also play a key role in mediating FHF differentiation. Indeed cardiac mesoderm differentiation is affected in the absence of Sox17 -a transcription factor required for maintenance of the definitive endoderm- and this is accompanied by the formation of a morphologically abnormal HT (***Pfister et al., 2011***). It remains, however, unclear whether this effect is secondary to an initial defect in foregut development that is observed in this mutant.

A recent study reported spontaneous calcium transients propagating laterally thought the cardiac crescent (***Tyser et al., 2016***). Left/Right (L/R) asymmetry therefore exists within the cardiac crescent, prior to any detectable cardiac contraction, and BMP/SMAD1 signaling in the lateral plate mesoderm may be involved in this asymmetry (***Furtado et al., 2008***). In our studies, however, we did not detect any L/R difference in cTnnT expression by whole-mount immunodetection or Nkx2.5GFP activation by live analysis in the cc.

Regarding the possible conservation of the temporal differentiation sequence described here, elegant experiments in zebrafish using a cardiac myosin light chain reporter line and a Kaede photoconversion assay, addressed the temporal order of cardiac differentiation in live embryos (***de Pater et al., 2009***; ***Liu and Stainier, 2012***). Two distinct phases of cardiomyocyte differentiation were also observed. During a first phase, cardiomyocytes were recruited first into the ventricle and atria at the venous pole. During a second phase, cardiomyocyte differentiation was observed at the arterial pole of the HT. These pulse-chase experiments, however, do not address whether cardiac differentiation is continuous or includes a differentiation-paused phase, so further studies will be required to establish the conservation of the observations made here for the mouse embryo.

Finally, an important question to address is the functional relevance of the three distinct phases described here; more specifically, what is the role of the observed differentiation pause. An interesting possibility is that this pause would be functionally related to the extensive morphogenetic events that transform the cardiac crescent into the HT. Our study demonstrates coordinated splanchnic mesoderm movements during this phase. These movements involve a very active antero-medial displacement of the splanchnic mesoderm surrounding the cc -mostly fated to the SHF-. This behavior of the splanchnic mesoderm appears essential for transforming the cc into a dorsally closed HT. Importantly, this displacement involves the sliding of the splanchnic layer over the endoderm, suggesting an active role of SHF precursors in this morphogenetic movement. Such displacement of the splanchnic mesoderm over the endoderm during cardiogenesis had been suggested by classical time-lapse studies in the chick embryo (**Dehaan, 1963**), and it is tempting to speculate that a similar phenomenon contributes to the incorporation of SHF cells to both poles of the HT at later stages of HT development (**van den Berg et al., 2009**; **Kelly et al., 2001**; **Zaffran et al., 2004**). These observations suggest that SHF cells do not represent just a reservoir of cardiac precursors but play a morphogenetic role essential for heart tube formation. The main consequence of the displacement of the splanchnic mesoderm layer over the endoderm is the medial convergence of the left and right frontiers between the cc and SHF to form the dorsal mesocardium and close the HT. An important consequence of the differentiation pause described here is the stability of the cc/SHF frontiers during these morphogenetic movements. This stability prevents further spreading of the differentiation wave from the cc into the SHF/splanchnic mesoderm, which could interfere the ability of the latter to efficiently displace over the endoderm. We therefore hypothesize that the stability of the cc/SHF frontiers – and thus the differentiation pause – would be essential to allow the effective displacement of SHF/splanchnic mesoderm and elicit HT formation. The temporal allocation of the morphogenetic phase after cc differentiation allows the formation of the HT while simultaneously providing an incipient cardiac function essential for the organization of embryonic circulation. This hypothesis poses a functional basis for the alternation of differentiation and morphogenesis phases during HT formation.

Our study applies whole-embryo live analysis of cardiac development at tissue level and with cellular resolution. We expect that extending this experimental approach will allow to further uncover unexpected and novel mechanisms of organogenesis. While limited attention had been paid so far to the temporal dynamics of differentiation during embryonic development, this is an essential aspect of organogenesis (**Gogendeau et al., 2015**; **Parchem et al., 2015**; **Yang et al., 2015**). Here, we show the relevance of differentiation timing regulation during heart tube formation and its coordination with morphogenesis at the tissue level. Further understanding of the molecular and cellular mechanisms underlying these phenomena will help us expanding pools of cardiac progenitors in vitro or directing them towards differentiation.

Materials and methods

Mouse strains

Mouse alleles used in the manuscript are listed including bibliographic references and allele identities at the 'Mouse Genome Informatics' data base (MGI, http://www.informatics.jax.org/). *Mesp1^{cre}* (**Saga et al., 1999**, MGI:2176467), *Isl1^{cre}* (**Cai et al., 2003**, MGI:3623159), *Nkx2.5^{cre}* (**Stanley et al., 2002**, MGI:2448972), *Rosa26Rtdtomato* (**Madisen et al., 2010**, MGI:3809524), *Rosa26RmTmG* (**Muzumdar et al., 2007**, MGI:3716464), *Nkx2.5eGFP* (**Wu et al., 2006**, MGI:5788423), *Polr2a^{CreERT2}* (*RERT*) (**Guerra et al., 2003**, MGI:3772332) and *C57BL/6* (Charles River). Mice were genotyped as previously described. All animal procedures were approved by the CNIC Animal Experimentation Ethics Committee, by the Community of Madrid (Ref. PROEX 220/15) and conformed to EU Directive 2010/63EU and Recommendation 2007/526/EC regarding the protection of animals used for experimental and other scientific purposes, enforced in Spanish law under Real Decreto 1201/2005.

Immunostaining and imaging

Embryos dissected in Dulbecco's modified Eagle's medium (DMEM, Invitrogen) were fixed overnight in 2% PFA at 4C, then permeabilized in PBST (PBS containing 0.1% Triton X-100) and blocked (5% goat serum). Embryos were incubated overnight at 4°C with antibodies diluted in PBST: mouse anti-

cTnnT (1:250, MS-295 Thermo Scientific), rabbit anti-PH3 (1:250, 06–570 Millipore), CD31 (553370 BD Pharmingen clone MEC 13.3), SMA (C6198 Sigma) and rabbit anti-Laminin1 (1:500, Sigma, L9393). After washing in freshly prepared PBST at 4°C, embryos were incubated with secondary antibodies (Molecular Probes, A21121, A21141, A11035) coupled to 488, 549 or 649 fluorophores as required at 1:250 and DAPI at 1:500 (Molecular Probes, D3571) overnight at 4°C. Before imaging, embryos were washed in PBST at room temperature and cleared with focus clear (Cell Explorer, FC-101) to enhance the transparency of the embryo. Confocal images were obtained on a SP8 Leica confocal microscope with a 20X oil objective (0.7 NA) at a 1024 × 1024 pixels dimension with a z-step of 2–4 µm. Embryos were systematically imaged throughout the entire heart tube from top to bottom.

3D reconstruction and volumetric measurement

For 3D rendering, fluorescent signal in confocal z-stacks was first segmented by setting intensity thresholds using the trainable Weka segmentation tool plugin available in Fiji (***Arganda-Carreras et al., 2017***; ***Schindelin et al., 2012***). The resulting z-stacks were then corrected manually on a slide-by-slide basis to eliminate segmentation mistakes. In case of the cTnnT immunofluorescence images (***Figure 1***), background signal from the yolk sack was manually masked. The volume of the cTnnT positive myocardium was then computed by multiplying the total segmented area by the z-stack interval using a custom Fiji macro. In the *Nkx2.5$^{cre/+}$; Rosa26tdtomato$^{+/-}$* and *Nkx2.5eGFP* embryos, fluorophore signal present in the endothelium, endocardium and endoderm cells was manually masked prior to segmentation (***Figure 1A***, ***Figure 1—figure supplement 1***, ***Figure 2B***, ***Figure 2—figure supplement 2A,A'*** and, ***Figure 6A''***). For 3D visualization of the 3D segmented image stacks, Imaris software (Bitplane) was used.

Embryo culture and two-photon live-imaging

Embryos were dissected at E7.5 in pre-equilibrated DMEM supplemented with 10% foetal bovine serum, 25 mM HEPES-NaOH (pH 7.2), penicillin (50µml21) and streptomycin (50mgml21). Embryos were staged on the basis of morphological criteria (supplementary Figure 1) (***Downs and Davies, 1993***; ***Lawson and Wilson, 2016***), and those between the bud and early somitogenesis stages were used for culture and time-lapse imaging. To track the early phase of cardiac differentiation and subsequent phases of morphogenesis, we used embryos at EHF to transversal HT stage. Embryos were cultured in 50% fresh rat serum, 48% DMEM without phenol red, 1% N-2 neuronal growth supplement (100X, Invitrogen 17502–048) and 1% B-27 supplement (50X Thermo Fisher Scientist 17504044) filter sterilised through a 0.2 mm filter. To hold embryos in position during time-lapse acquisition, we made special plastic holders with holes of different diameters (0.5–3 mm) to ensure a good fit of embryos similarly to the traps developed by ***Nonaka, 2009***, ***Nonaka et al. (2002)***. Embryos were mounted with their anterior side facing up. To avoid evaporation, the medium was covered with mineral oil (Sigma-Aldrich; M8410). Before starting the time-lapse acquisition, embryos were first pre-cultured for at least 2 hr in the microscopy culture set up. The morphology of the embryo was then carefully monitored and if the embryos appeared unhealthy or rotate and move, they were discarded, otherwise, time-lapse acquisition was performed. For the acquisition, we used the Zeiss LSM780 equipped with a 5% CO_2 incubator and a heating chamber maintaining 37°C. The objective lens used was a 20X(NA = 1) dipping objective, which allowed a long working distance for imaging mouse embryos and tissues. A MaiTai laser line at 1000 nm was used for two-channel two-photon imaging. Acquisition was done using Zen software (Zeiss). Typical image settings were: output power: 250 mW, pixel dwell time: 7µs, line averaging: two and image dimension: 610 × 610 µm (1024 × 1024 pixels). To maximize the chance of covering the entire heart tube during long-term time lapse videos, we allowed 150–200 µm of free space between the objective and the embryo at the beginning of the recording.

Cell labeling, 3D tracking and GFP intensity measurement

For labeling single cells, tamoxifen was administered by oral gavage (2–4 mg/mL) in *RERT;Rosa26R-tdtomato* (cell tracking) or *RERT;Rosa26RmTmG* mice (cell shape study) at E7. Cell shape measurements were done on single cells, imaged in mosaic-labeled, fixed and immunostained embryos and analyzed with Fiji software (***Figure 2D,E***). Tracking of tdtomato-labeled cells was done on single cells

located within the cardiogenic mesoderm -excluding endothelial, pericardial and endodermal cells- and their GFP intensity was measured over time. To track cells manually in 4D stacks, the MTrackJ Fiji plugin (***Meijering et al., 2012***) was used. A local square cursor (25 × 25 pixels) on the cell of interest snaps according to a bright centroid feature on a slice-by-slice basis. Only tracks lasting for the entire length of the video were kept. When an ambiguity arises in the tracking between consecutive time points, the track was discarded. Tracks split at cell divisions. A cell division event is normally clearly distinguishable over at least two time points. In case one of the two daughter cells is not tractable, the other daughter cell is still tracked. Each track is assigned an ID number and excel files with all the tracks coordinates in x, y, z and t was generated. Coordinates of each track were converted into 8-bit 4D images using a custom Fiji macro in which each cell was represented by a sphere of specific pixel intensity, from 1 to 255, while pixels corresponding to background were set to zero. The 4D images were then opened with Imaris to perform visualization of the 3D trajectories of each cell using the 'spots' tool, where each object were identified according to pixel intensity. GFP intensity measurement is performed by segmentation of cell shape. A Gaussian filter whose radius is adjusted to the typical size of a cell was first applied, followed by a Laplacian filter. The resulting 32 bits image was next converted to a mask by thresholding. When objects touched each other, a watershed on the binary mask and manual corrections was applied. Each segmented cell was checked and tracked manually for accuracy. In ***Figure 3B'*** nuclei segmentation was performed manually. The mean GFP signal intensity of the segmented objects was then measured using the 'analyze particle' tool in Fiji. To quantify the GFP level of tracked cells through time, four to five successive time points were arbitrarily chosen in each video (***Figure 5F***, ***Figure 6C,D*** and ***Figure 5—figure supplement 1C***) except in ***Figure 5D*** and ***Figure 6I***, where GFP intensity level was measured in every time point. Background intensities were measured in neural tube cells, which are known to be negative for GFP and cTnnT. Tables containing ID number of tracked cells and GFP intensities were generated and plotted using Prism statistical software.

Statistical analysis

For comparisons of two groups, a Mann–Whitney U-test was used using Prism statistical software. To find a correlation between GFP and cTnnT levels of 0.8 with an alpha-level f 0.05 and a power of 0.2 at least 10 cells per embryo were required (***Figure 3D*** and ***Figure 3—figure supplement 2C***). Many more cells were computed for each experiment. The linear fit was done using 'lm' function from R statistical software (https://www.r-project.org/). To calculate the average speed of splanchnic mesoderm displacement, the shortest distance between the left and right splanchnic mesoderm was calculated in two z-level, using the measure tool in Fiji, and the variation in this distance by time unit was divided by 2, to determine the speed of movement of each sliding side of the splanchnic mesoderm.

Acknowledgements

We thank the CNIC Microscopy unit for help with the live confocal analysis, Fatima Sanchez Cabo for help with the statistical analyses and Florencia Cavodeassi, Miguel Manzanares, Briane Laruy and members of the Torres lab for helpful comments on the manuscript. This work was supported by grants BFU2015-71519-P, BFU2015-70193-REDT and RD16/0011/0019 (ISCIII) from the Spanish Ministry of Economy, Industry and Competitiveness (MEIC). KI was supported by a Human Frontiers Science Program (LT000609/2015) and EMBO (ATL1275-2014) postdoctoral fellowships. The CNIC is supported by the Spanish MEIC and the Pro CNIC Foundation, and is a Severo Ochoa Center of Excellence (MINECO award SEV-2015–0505). The authors declare no conflicts of interest.

Additional information

Funding

Funder	Grant reference number	Author
Ministerio de Economía y Competitividad	BFU2015-71519-P	Miguel Torres

Instituto de Salud Carlos III	RD16/0011/0019	Miguel Torres
European Molecular Biology Organization	ATL1275-2014	Kenzo Ivanovitch
Human Frontier Science Program	LT000609/2015	Kenzo Ivanovitch
Ministerio de Economía y Competitividad	BFU2015-70193-REDT	Miguel Torres
Ministerio de Economía y Competitividad	SEV-2015-0505	Miguel Torres

The funders had no role in study design, data collection and interpretation, or the decision to submit the work for publication.

Author contributions

Kenzo Ivanovitch, Conceptualization, Data curation, Formal analysis, Investigation, Methodology, Writing—original draft, Writing—review and editing; Susana Temiño, Methodology, Provided technical help; Miguel Torres, Conceptualization, Supervision, Funding acquisition, Writing—review and editing

Author ORCIDs

Kenzo Ivanovitch http://orcid.org/0000-0003-4706-7686
Miguel Torres http://orcid.org/0000-0003-0906-4767

Ethics

Animal experimentation: All animal procedures were approved by the CNIC Animal Experimentation Ethics Committee, by the Community of Madrid (Ref. PROEX 220/15) and conformed to EU Directive 2010/63EU and Recommendation 2007/526/EC regarding the protection of animals used for experimental and other scientific purposes, enforced in Spanish law under Real Decreto 1201/2005.

Decision letter and Author response

Decision letter https://doi.org/10.7554/eLife.30668.057
Author response https://doi.org/10.7554/eLife.30668.058

Additional files

Supplementary files

- Transparent reporting form

DOI: https://doi.org/10.7554/eLife.30668.055

References

Abu-Issa R, Waldo K, Kirby ML. 2004. Heart fields: one, two or more? *Developmental Biology* **272**:281–285. DOI: https://doi.org/10.1016/j.ydbio.2004.05.016, PMID: 15282148

Abu-Issa R. 2014. Heart fields: spatial polarity and temporal dynamics. *The Anatomical Record* **297**:175–182. DOI: https://doi.org/10.1002/ar.22831, PMID: 24443184

Ai D, Fu X, Wang J, Lu MF, Chen L, Baldini A, Klein WH, Martin JF. 2007. Canonical Wnt signaling functions in second heart field to promote right ventricular growth. *PNAS* **104**:9319–9324. DOI: https://doi.org/10.1073/pnas.0701212104, PMID: 17519332

Arganda-Carreras I, Kaynig V, Rueden C, Eliceiri KW, Schindelin J, Cardona A, Sebastian Seung H. 2017. Trainable Weka Segmentation: a machine learning tool for microscopy pixel classification. *Bioinformatics* **33**:2424–2426. DOI: https://doi.org/10.1093/bioinformatics/btx180, PMID: 28369169

Biben C, Weber R, Kesteven S, Stanley E, McDonald L, Elliott DA, Barnett L, Köentgen F, Robb L, Feneley M, Harvey RP. 2000. Cardiac septal and valvular dysmorphogenesis in mice heterozygous for mutations in the homeobox gene Nkx2-5. *Circulation Research* **87**:888–895. DOI: https://doi.org/10.1161/01.RES.87.10.888, PMID: 11073884

Boothe T, Hilbert L, Heide M, Berninger L, Huttner WB, Zaburdaev V, Vastenhouw NL, Myers EW, Drechsel DN, Rink JC. 2017. A tunable refractive index matching medium for live imaging cells, tissues and model organisms. *eLife* **6**–351. DOI: https://doi.org/10.7554/eLife.27240, PMID: 28708059

Brade T, Gessert S, Kühl M, Pandur P. 2007. The amphibian second heart field: Xenopus islet-1 is required for cardiovascular development. *Developmental Biology* **311**:297–310. DOI: https://doi.org/10.1016/j.ydbio.2007.08.004, PMID: 17900553

Buckingham M, Meilhac S, Zaffran S. 2005. Building the mammalian heart from two sources of myocardial cells. *Nature Reviews Genetics* **6**:826–837. DOI: https://doi.org/10.1038/nrg1710, PMID: 16304598

Cai CL, Liang X, Shi Y, Chu PH, Pfaff SL, Chen J, Evans S. 2003. Isl1 identifies a cardiac progenitor population that proliferates prior to differentiation and contributes a majority of cells to the heart. *Developmental Cell* **5**:877–889. DOI: https://doi.org/10.1016/S1534-5807(03)00363-0, PMID: 14667410

Chen CM, Miranda AM, Bub G, Srinivas S. 2014. Detecting cardiac contractile activity in the early mouse embryo using multiple modalities. *Frontiers in Physiology* **5**:508. DOI: https://doi.org/10.3389/fphys.2014.00508, PMID: 25610399

Christoffels VM, Habets PE, Franco D, Campione M, de Jong F, Lamers WH, Bao ZZ, Palmer S, Biben C, Harvey RP, Moorman AF. 2000. Chamber formation and morphogenesis in the developing mammalian heart. *Developmental Biology* **223**:266–278. DOI: https://doi.org/10.1006/dbio.2000.9753, PMID: 10882515

Christoffels VM, Mommersteeg MT, Trowe MO, Prall OW, de Gier-de Vries C, Soufan AT, Bussen M, Schuster-Gossler K, Harvey RP, Moorman AF, Kispert A. 2006. Formation of the venous pole of the heart from an Nkx2-5-negative precursor population requires Tbx18. *Circulation Research* **98**:1555–1563. DOI: https://doi.org/10.1161/01.RES.0000227571.84189.65, PMID: 16709898

de Boer BA, van den Berg G, de Boer PA, Moorman AF, Ruijter JM. 2012. Growth of the developing mouse heart: an interactive qualitative and quantitative 3D atlas. *Developmental Biology* **368**:203–213. DOI: https://doi.org/10.1016/j.ydbio.2012.05.001, PMID: 22617458

de Pater E, Clijsters L, Marques SR, Lin YF, Garavito-Aguilar ZV, Yelon D, Bakkers J. 2009. Distinct phases of cardiomyocyte differentiation regulate growth of the zebrafish heart. *Development* **136**:1633–1641. DOI: https://doi.org/10.1242/dev.030924, PMID: 19395641

Dehaan RL. 1963. Migration patterns of the precardiac mesoderm in the early chick embrvo. *Experimental Cell Research* **29**:544–560. DOI: https://doi.org/10.1016/S0014-4827(63)80016-6, PMID: 14026475

Devine WP, Wythe JD, George M, Koshiba-Takeuchi K, Bruneau BG. 2014. Early patterning and specification of cardiac progenitors in gastrulating mesoderm. *eLife* **3**:e03848. DOI: https://doi.org/10.7554/eLife.03848, PMID: 25296024

Diogo R, Kelly RG, Christiaen L, Levine M, Ziermann JM, Molnar JL, Noden DM, Tzahor E. 2015. A new heart for a new head in vertebrate cardiopharyngeal evolution. *Nature* **520**:466–473. DOI: https://doi.org/10.1038/nature14435, PMID: 25903628

Downs KM, Davies T. 1993. Staging of gastrulating mouse embryos by morphological landmarks in the dissecting microscope. *Development* **118**:1255–1266. PMID: 8269852

Evans SM, Yelon D, Conlon FL, Kirby ML. 2010. Myocardial lineage development. *Circulation Research* **107**:1428–1444. DOI: https://doi.org/10.1161/CIRCRESAHA.110.227405, PMID: 21148449

Francou A, Saint-Michel E, Mesbah K, Kelly RG. 2014. TBX1 regulates epithelial polarity and dynamic basal filopodia in the second heart field. *Development* **141**:4320–4331. DOI: https://doi.org/10.1242/dev.115022, PMID: 25371366

Furtado MB, Solloway MJ, Jones VJ, Costa MW, Biben C, Wolstein O, Preis JI, Sparrow DB, Saga Y, Dunwoodie SL, Robertson EJ, Tam PP, Harvey RP. 2008. BMP/SMAD1 signaling sets a threshold for the left/right pathway in lateral plate mesoderm and limits availability of SMAD4. *Genes & Development* **22**:3037–3049. DOI: https://doi.org/10.1101/gad.1682108, PMID: 18981480

Galli D, Domínguez JN, Zaffran S, Munk A, Brown NA, Buckingham ME. 2008. Atrial myocardium derives from the posterior region of the second heart field, which acquires left-right identity as Pitx2c is expressed. *Development* **135**:1157–1167. DOI: https://doi.org/10.1242/dev.014563, PMID: 18272591

Gogendeau D, Siudeja K, Gambarotto D, Pennetier C, Bardin AJ, Basto R. 2015. Aneuploidy causes premature differentiation of neural and intestinal stem cells. *Nature Communications* **6**:8894. DOI: https://doi.org/10.1038/ncomms9894, PMID: 26573328

Guerra C, Mijimolle N, Dhawahir A, Dubus P, Barradas M, Serrano M, Campuzano V, Barbacid M. 2003. Tumor induction by an endogenous K-ras oncogene is highly dependent on cellular context. *Cancer Cell* **4**:111–120. DOI: https://doi.org/10.1016/S1535-6108(03)00191-0, PMID: 12957286

Jain R, Li D, Gupta M, Manderfield LJ, Ifkovits JL, Wang Q, Liu F, Liu Y, Poleshko A, Padmanabhan A, Raum JC, Li L, Morrisey EE, Lu MM, Won KJ, Epstein JA. 2015. HEART DEVELOPMENT. Integration of Bmp and Wnt signaling by Hopx specifies commitment of cardiomyoblasts. *Science* **348**:aaa6071. DOI: https://doi.org/10.1126/science.aaa6071, PMID: 26113728

Kelly RG, Brown NA, Buckingham ME. 2001. The arterial pole of the mouse heart forms from Fgf10-expressing cells in pharyngeal mesoderm. *Developmental Cell* **1**:435–440. DOI: https://doi.org/10.1016/S1534-5807(01)00040-5, PMID: 11702954

Kelly RG, Buckingham ME, Moorman AF. 2014. Heart fields and cardiac morphogenesis. *Cold Spring Harbor Perspectives in Medicine* **4**:a015750. DOI: https://doi.org/10.1101/cshperspect.a015750, PMID: 25274757

Klaus A, Saga Y, Taketo MM, Tzahor E, Birchmeier W. 2007. Distinct roles of Wnt/beta-catenin and Bmp signaling during early cardiogenesis. *PNAS* **104**:18531–18536. DOI: https://doi.org/10.1073/pnas.0703113104, PMID: 18000065

Kwon C, Arnold J, Hsiao EC, Taketo MM, Conklin BR, Srivastava D. 2007. Canonical Wnt signaling is a positive regulator of mammalian cardiac progenitors. *PNAS* **104**:10894–10899. DOI: https://doi.org/10.1073/pnas.0704044104, PMID: 17576928

Laugwitz KL, Moretti A, Lam J, Gruber P, Chen Y, Woodard S, Lin LZ, Cai CL, Lu MM, Reth M, Platoshyn O, Yuan JX, Evans S, Chien KR. 2005. Postnatal isl1+ cardioblasts enter fully differentiated cardiomyocyte lineages. *Nature* **433**:647–653. DOI: https://doi.org/10.1038/nature03215, PMID: 15703750

Lawson KA, Wilson V. 2016. 3 – A revised staging of mouse development before organogenesis. In: Baldock R, Bard J, Davidson D, Morriss-Kay G (Eds). *Kaufman's Atlas of Mouse Development Supplement*. Academic Press.

Lescroart F, Chabab S, Lin X, Rulands S, Paulissen C, Rodolosse A, Auer H, Achouri Y, Dubois C, Bondue A, Simons BD, Blanpain C. 2014. Early lineage restriction in temporally distinct populations of Mesp1 progenitors during mammalian heart development. *Nature Cell Biology* **16**:829–840. DOI: https://doi.org/10.1038/ncb3024, PMID: 25150979

Lescroart F, Hamou W, Francou A, Théveniau-Ruissy M, Kelly RG, Buckingham M. 2015. Clonal analysis reveals a common origin between nonsomite-derived neck muscles and heart myocardium. *PNAS* **112**:1446–1451. DOI: https://doi.org/10.1073/pnas.1424538112, PMID: 25605943

Lescroart F, Kelly RG, Le Garrec JF, Nicolas JF, Meilhac SM, Buckingham M. 2010. Clonal analysis reveals common lineage relationships between head muscles and second heart field derivatives in the mouse embryo. *Development* **137**:3269–3279. DOI: https://doi.org/10.1242/dev.050674, PMID: 20823066

Lien CL, Wu C, Mercer B, Webb R, Richardson JA, Olson EN. 1999. Control of early cardiac-specific transcription of Nkx2-5 by a GATA-dependent enhancer. *Development* **126**:75–84. PMID: 9834187

Linask KK, Knudsen KA, Gui YH. 1997. N-cadherin-catenin interaction: necessary component of cardiac cell compartmentalization during early vertebrate heart development. *Developmental Biology* **185**:148–164. DOI: https://doi.org/10.1006/dbio.1997.8570, PMID: 9187080

Liu J, Stainier DY. 2012. Zebrafish in the study of early cardiac development. *Circulation Research* **110**:870–874. DOI: https://doi.org/10.1161/CIRCRESAHA.111.246504, PMID: 22427324

Ma Q, Zhou B, Pu WT. 2008. Reassessment of Isl1 and Nkx2-5 cardiac fate maps using a Gata4-based reporter of Cre activity. *Developmental Biology* **323**:98–104. DOI: https://doi.org/10.1016/j.ydbio.2008.08.013, PMID: 18775691

Madisen L, Zwingman TA, Sunkin SM, Oh SW, Zariwala HA, Gu H, Ng LL, Palmiter RD, Hawrylycz MJ, Jones AR, Lein ES, Zeng H. 2010. A robust and high-throughput Cre reporting and characterization system for the whole mouse brain. *Nature Neuroscience* **13**:133–140. DOI: https://doi.org/10.1038/nn.2467, PMID: 20023653

Marvin MJ, Di Rocco G, Gardiner A, Bush SM, Lassar AB. 2001. Inhibition of Wnt activity induces heart formation from posterior mesoderm. *Genes & Development* **15**:316–327. DOI: https://doi.org/10.1101/gad.855501, PMID: 11159912

Meijering E, Dzyubachyk O, Smal I. 2012. Methods for cell and particle tracking. *Methods in Enzymology* **504**:183–200. DOI: https://doi.org/10.1016/B978-0-12-391857-4.00009-4, PMID: 22264535

Meilhac SM, Esner M, Kelly RG, Nicolas JF, Buckingham ME. 2004a. The clonal origin of myocardial cells in different regions of the embryonic mouse heart. *Developmental Cell* **6**:685–698. DOI: https://doi.org/10.1016/S1534-5807(04)00133-9, PMID: 15130493

Meilhac SM, Esner M, Kerszberg M, Moss JE, Buckingham ME. 2004b. Oriented clonal cell growth in the developing mouse myocardium underlies cardiac morphogenesis. *The Journal of Cell Biology* **164**:97–109. DOI: https://doi.org/10.1083/jcb.200309160, PMID: 14709543

Mjaatvedt CH, Nakaoka T, Moreno-Rodriguez R, Norris RA, Kern MJ, Eisenberg CA, Turner D, Markwald RR. 2001. The outflow tract of the heart is recruited from a novel heart-forming field. *Developmental Biology* **238**:97–109. DOI: https://doi.org/10.1006/dbio.2001.0409, PMID: 11783996

Moorman AF, Christoffels VM, Anderson RH, van den Hoff MJ. 2007. The heart-forming fields: one or multiple? *Philosophical Transactions of the Royal Society B: Biological Sciences* **362**:1257–1265. DOI: https://doi.org/10.1098/rstb.2007.2113, PMID: 17581808

Moretti A, Caron L, Nakano A, Lam JT, Bernshausen A, Chen Y, Qyang Y, Bu L, Sasaki M, Martin-Puig S, Sun Y, Evans SM, Laugwitz KL, Chien KR. 2006. Multipotent embryonic isl1+ progenitor cells lead to cardiac, smooth muscle, and endothelial cell diversification. *Cell* **127**:1151–1165. DOI: https://doi.org/10.1016/j.cell.2006.10.029, PMID: 17123592

Muzumdar MD, Tasic B, Miyamichi K, Li L, Luo L. 2007. A global double-fluorescent Cre reporter mouse. *Genesis* **45**:593–605. DOI: https://doi.org/10.1002/dvg.20335, PMID: 17868096

Nonaka S, Shiratori H, Saijoh Y, Hamada H. 2002. Determination of left-right patterning of the mouse embryo by artificial nodal flow. *Nature* **418**:96–99. DOI: https://doi.org/10.1038/nature00849, PMID: 12097914

Nonaka S. 2009. Modification of mouse nodal flow by applying artificial flow. *Methods in Cell Biology* **91**:287–297. DOI: https://doi.org/10.1016/S0091-679X(08)91015-3, PMID: 20409792

Parchem RJ, Moore N, Fish JL, Parchem JG, Braga TT, Shenoy A, Oldham MC, Rubenstein JL, Schneider RA, Blelloch R. 2015. miR-302 is required for timing of neural differentiation, neural tube closure, and embryonic viability. *Cell Reports* **12**:760–773. DOI: https://doi.org/10.1016/j.celrep.2015.06.074, PMID: 26212322

Pfister S, Jones VJ, Power M, Truisi GL, Khoo PL, Steiner KA, Kanai-Azuma M, Kanai Y, Tam PP, Loebel DA. 2011. Sox17-dependent gene expression and early heart and gut development in Sox17-deficient mouse embryos. *The International Journal of Developmental Biology* **55**:45–58. DOI: https://doi.org/10.1387/ijdb.103158sp, PMID: 21305474

Prall OW, Menon MK, Solloway MJ, Watanabe Y, Zaffran S, Bajolle F, Biben C, McBride JJ, Robertson BR, Chaulet H, Stennard FA, Wise N, Schaft D, Wolstein O, Furtado MB, Shiratori H, Chien KR, Hamada H, Black BL, Saga Y, et al. 2007. An Nkx2-5/Bmp2/Smad1 negative feedback loop controls heart progenitor specification and proliferation. *Cell* **128**:947–959. DOI: https://doi.org/10.1016/j.cell.2007.01.042, PMID: 17350578

Qyang Y, Martin-Puig S, Chiravuri M, Chen S, Xu H, Bu L, Jiang X, Lin L, Granger A, Moretti A, Caron L, Wu X, Clarke J, Taketo MM, Laugwitz KL, Moon RT, Gruber P, Evans SM, Ding S, Chien KR. 2007. The renewal and differentiation of Isl1+ cardiovascular progenitors are controlled by a Wnt/beta-catenin pathway. *Cell Stem Cell* **1**:165–179. DOI: https://doi.org/10.1016/j.stem.2007.05.018, PMID: 18371348

Ramsbottom SA, Sharma V, Rhee HJ, Eley L, Phillips HM, Rigby HF, Dean C, Chaudhry B, Henderson DJ. 2014. Vangl2-regulated polarisation of second heart field-derived cells is required for outflow tract lengthening during cardiac development. *PLoS Genetics* **10**:e1004871. DOI: https://doi.org/10.1371/journal.pgen.1004871, PMID: 25521757

Saga Y, Hata N, Kobayashi S, Magnuson T, Seldin MF, Taketo MM. 1996. MesP1: a novel basic helix-loop-helix protein expressed in the nascent mesodermal cells during mouse gastrulation. *Development* **122**:2769–2778. PMID: 8787751

Saga Y, Miyagawa-Tomita S, Takagi A, Kitajima S, Miyazaki J, Inoue T. 1999. MesP1 is expressed in the heart precursor cells and required for the formation of a single heart tube. *Development* **126**:3437–3447. PMID: 10393122

Schindelin J, Arganda-Carreras I, Frise E, Kaynig V, Longair M, Pietzsch T, Preibisch S, Rueden C, Saalfeld S, Schmid B, Tinevez JY, White DJ, Hartenstein V, Eliceiri K, Tomancak P, Cardona A. 2012. Fiji: an open-source platform for biological-image analysis. *Nature Methods* **9**:676–682. DOI: https://doi.org/10.1038/nmeth.2019, PMID: 22743772

Sinha T, Wang B, Evans S, Wynshaw-Boris A, Wang J. 2012. Disheveled mediated planar cell polarity signaling is required in the second heart field lineage for outflow tract morphogenesis. *Developmental Biology* **370**:135–144. DOI: https://doi.org/10.1016/j.ydbio.2012.07.023, PMID: 22841628

Sizarov A, Ya J, de Boer BA, Lamers WH, Christoffels VM, Moorman AF. 2011. Formation of the building plan of the human heart: morphogenesis, growth, and differentiation. *Circulation* **123**:1125–1135. DOI: https://doi.org/10.1161/CIRCULATIONAHA.110.980607, PMID: 21403123

Später D, Abramczuk MK, Buac K, Zangi L, Stachel MW, Clarke J, Sahara M, Ludwig A, Chien KR. 2013. A HCN4 + cardiomyogenic progenitor derived from the first heart field and human pluripotent stem cells. *Nature Cell Biology* **15**:1098–1106. DOI: https://doi.org/10.1038/ncb2824, PMID: 23974038

Stanley EG, Biben C, Elefanty A, Barnett L, Koentgen F, Robb L, Harvey RP. 2002. Efficient Cre-mediated deletion in cardiac progenitor cells conferred by a 3'UTR-ires-Cre allele of the homeobox gene Nkx2-5. *The International Journal of Developmental Biology* **46**:431–439. PMID: 12141429

Tirosh-Finkel L, Zeisel A, Brodt-Ivenshitz M, Shamai A, Yao Z, Seger R, Domany E, Tzahor E. 2010. BMP-mediated inhibition of FGF signaling promotes cardiomyocyte differentiation of anterior heart field progenitors. *Development* **137**:2989–3000. DOI: https://doi.org/10.1242/dev.051649, PMID: 20702560

Tyser RC, Miranda AM, Chen CM, Davidson SM, Srinivas S, Riley PR. 2016. Calcium handling precedes cardiac differentiation to initiate the first heartbeat. *eLife* **5**:e17113. DOI: https://doi.org/10.7554/eLife.17113, PMID: 27725084

Ueno S, Weidinger G, Osugi T, Kohn AD, Golob JL, Pabon L, Reinecke H, Moon RT, Murry CE. 2007. Biphasic role for Wnt/beta-catenin signaling in cardiac specification in zebrafish and embryonic stem cells. *PNAS* **104**:9685–9690. DOI: https://doi.org/10.1073/pnas.0702859104, PMID: 17522258

van den Berg G, Abu-Issa R, de Boer BA, Hutson MR, de Boer PA, Soufan AT, Ruijter JM, Kirby ML, van den Hoff MJ, Moorman AF. 2009. A caudal proliferating growth center contributes to both poles of the forming heart tube. *Circulation Research* **104**:179–188. DOI: https://doi.org/10.1161/CIRCRESAHA.108.185843, PMID: 19059840

Waldo KL, Kumiski DH, Wallis KT, Stadt HA, Hutson MR, Platt DH, Kirby ML. 2001. Conotruncal myocardium arises from a secondary heart field. *Development* **128**:3179–3188. PMID: 11688566

Wu SM, Fujiwara Y, Cibulsky SM, Clapham DE, Lien CL, Schultheiss TM, Orkin SH. 2006. Developmental origin of a bipotential myocardial and smooth muscle cell precursor in the mammalian heart. *Cell* **127**:1137–1150. DOI: https://doi.org/10.1016/j.cell.2006.10.028, PMID: 17123591

Yang SL, Yang M, Herrlinger S, Liang C, Lai F, Chen JF. 2015. MiR-302/367 regulate neural progenitor proliferation, differentiation timing, and survival in neurulation. *Developmental Biology* **408**:140–150. DOI: https://doi.org/10.1016/j.ydbio.2015.09.020, PMID: 26441343

Yuan S, Schoenwolf GC. 2000. Islet-1 marks the early heart rudiments and is asymmetrically expressed during early rotation of the foregut in the chick embryo. *The Anatomical Record* **260**:204–207. DOI: https://doi.org/10.1002/1097-0185(20001001)260:2<204::AID-AR90>3.0.CO;2-5, PMID: 10993956

Zaffran S, Kelly RG, Meilhac SM, Buckingham ME, Brown NA. 2004. Right ventricular myocardium derives from the anterior heart field. *Circulation Research* **95**:261–268. DOI: https://doi.org/10.1161/01.RES.0000136815.73623.BE, PMID: 15217909